

# A FULL APPROXIMATION SCHEME MULTILEVEL METHOD FOR NONLINEAR VARIATIONAL INEQUALITIES\*

ED BUELER<sup>†</sup> AND PATRICK E. FARRELL<sup>‡</sup>

**Abstract.** We present the *full approximation scheme constraint decomposition* (FASCD) multilevel method for solving variational inequalities (VIs). FASCD is a joint extension of both the full approximation scheme (FAS) multigrid technique for nonlinear partial differential equations, due to A. Brandt, and the constraint decomposition (CD) method introduced by X.-C. Tai for VIs arising in optimization. We extend the CD idea by exploiting the telescoping nature of certain subset decompositions arising from multilevel mesh hierarchies. When a reduced-space (active set) Newton method is applied as a smoother, with work proportional to the number of unknowns on a given mesh level, FASCD V-cycles exhibit nearly mesh-independent convergence rates. The full multigrid cycle version is an optimal solver. The example problems include differential operators which are symmetric linear, nonsymmetric linear, and nonlinear, in unilateral and bilateral VI problems.

**Key words.** multigrid, variational inequalities, full approximation scheme, constraint decomposition

**MSC codes.** 65K15, 35M86, 90C33

**1. Introduction.** The constraint decomposition (CD) methods of Tai [32] are designed to solve variational inequality (VI) problems arising as the Karush–Kuhn–Tucker optimality conditions for the minimization of a convex functional over a convex set. In a finite element (FE) context, these methods converge for multilevel and domain decompositions. The multilevel CD method has almost grid-independent error bounds, and near-optimal complexity, for elliptic, linear obstacle problems [32, Subsection 5.4], [23, Theorem 4.6], but returns to the finest mesh are required when evaluating functions on coarse levels.

Here we extend Tai’s multilevel CD method by replacing the coarser-level corrections with a full approximation scheme (FAS; [5, 8]) approach. Specifically, our *full approximation scheme constraint decomposition* (FASCD) method enjoys the following advantages:

- (i) The FAS coarse corrections are adapted for general VI problems. The method requires neither an objective function nor linearity of the residual.
- (ii) Box constraints, i.e. both upper and lower obstacles, are allowed. (However, other convex admissible sets are not supported.)
- (iii) The method is strictly admissible, and so can be applied even if the residual operator is defined only on those functions which satisfy the constraints.
- (iv) The work at each level is proportional to the number of degrees of freedom on that level. Coarser-level evaluations do not require finest-level information.
- (v) V-cycles (Algorithm 6.1) and full multigrid (FMG; [34]) cycles (Algorithm 7.1) are implemented.

---

\*Draft January 24, 2024.

**Funding:** EB was supported by a Faculty Development Travel Award from United Academics, University of Alaska Fairbanks, and thanks Max Heldman for helpful comments. PEF was supported by the Engineering and Physical Sciences Research Council [EPSRC grants EP/R029423/1 and EP/W026163/1]. This work used the ARCHER2 UK National Supercomputing Service [www.archer2.ac.uk](http://www.archer2.ac.uk). PEF thanks Lawrence Mitchell for advice on implementation, and Jack D. Betteridge for assistance with running Example 8.4.

<sup>†</sup>Department of Mathematics and Statistics, University of Alaska Fairbanks, USA ([elbueler@alaska.edu](mailto:elbueler@alaska.edu)).

<sup>‡</sup>Mathematical Institute, University of Oxford, Oxford, UK ([patrick.farrell@maths.ox.ac.uk](mailto:patrick.farrell@maths.ox.ac.uk)).

- (vi) We identify a “telescoping” subset property, which is exploited on the up-smoothing side of a V-cycle, yielding better performance.
- (vii) The method is smoother-agnostic.
- (viii) Using a (mesh-dependent) reduced-space Newton method [3] as the smoother, in Section 8 we demonstrate that application of FMG is an optimal solver.

Prior multilevel algorithms for VIs have significant limitations compared to the FASCD framework. Listed chronologically, here are some comparisons:

- The projected full approximation scheme (PFAS) algorithm of Brandt & Cryer [6] applies to linear complementarity problems and it uses projected (truncated) Gauss–Seidel smoothers. While our method reduces to general, nonlinear FAS for PDEs when the inequality constraints are removed, PFAS reduces to linear multigrid.
- The multilevel CD iteration of Tai [32] is formulated in terms of an objective function; as stated it only applies to optimization-type problems. Furthermore, each of its coarser-level problems refers to the finest-level discretization. FASCD is both more general, as it applies to non-variational monotone operators (Section 2), and more efficient on each coarser level.
- The last-mentioned limitation of the [32] method is removed by Gräser & Kornhuber’s [23, Algorithm 4.2] reformulation using defect constraints and monotone injection operators. We adopt these techniques; see Section 5 below. However, the monotone multigrid methods of Kornhuber and co-authors [23, 30] appear to be formulated only with Gauss–Seidel type smoothers, and may have been applied only to optimization-type VI problems [27, for example]. Furthermore, unlike the fastest variants of monotone multigrid, no zeroing of the basis functions associated with the active set (truncation) is employed in FASCD, and this simplifies the implementation. FASCD coarse grid corrections can indeed update the finest-level active set, and the numerical evidence indicates that FASCD coarse corrections are effective even when the coarse meshes are far too coarse to resolve the active set. On a problem with a complicated coincidence set, for which truncated Newton/monotone multigrid methods were apparently designed [23, problem 7.1.1], the performance of FASCD is at least as good (Example 8.1).
- Another work which combines FAS and VIs is [25], but the problems solved, and the approach, are completely different. For an optimal control problem with an elliptic VI constraint, [25] applies FAS to a system of PDEs derived from penalizing the VI and the control constraints; their FAS algorithm is not applied to the VI itself while ours is.

In our experiments, FASCD V-cycles exhibit essentially the same mesh-independent convergence rates for VI problems that FAS multigrid V-cycles exhibit for the corresponding unconstrained PDE problems. In fact, the FMG results in Section 8 show near-textbook multigrid efficiency, yielding solutions within discretization error in work comparable to a relatively few smoother sweeps on the finest-level mesh [7]. We see this performance for classical (unilateral, Laplacian) obstacle problems,  $p$ -Laplacian obstacle problems, and box-constrained advection-diffusion equations. Furthermore, V-cycle results are largely insensitive to the geometric complexity of the coincidence set and free boundary.

All iterates in FASCD, on all mesh levels, are admissible, and thus the nonlinear operator in the VI needs only be defined for admissible states. For example, we solve an ice sheet geometry problem (Example 2.6) in which the flow formulas are only meaningful for surface elevation iterates that do not penetrate the bed-

rock. (Non-admissible methods, including semi-smooth methods [3], would require unnatural modifications of the operator formula.) The FASCD FMG cycle solves this low-regularity problem, in which the solution gradient is unbounded at the free boundary, optimally; see Example 8.4. Our results on this Example also demonstrate the parallel weak scaling [11] of our implementation.

The paper is organized as follows. In Section 2 we recall the theory of coercive and monotone VIs, and describe several motivating examples. Section 3 reviews CDs and their induced iterations. Section 4 sets up multilevel FE hierarchies, and then Section 5 implements the CD method using defect constraints which are generated by monotone injection. In Section 5 we also propose a new understanding of telescoping sets for up-smoothing, based on an “incomplete” CD and an associated iteration. Section 6 then states the FASCD V-cycle, and Section 7 addresses practical implementation including convergence criteria and the FMG cycle. Section 8 gives numerical results from our open source Python/Firedrake [31] implementation.

**2. Variational inequalities.** Let  $\mathcal{V}$  be a real reflexive Banach space with norm  $\|\cdot\|$  and topological dual space  $\mathcal{V}'$ . Denote the dual pairing of  $\phi \in \mathcal{V}'$  and  $v \in \mathcal{V}$  by  $\langle \phi, v \rangle = \phi(v)$ , and define the (Banach space) norm on  $\mathcal{V}'$  by  $\|\phi\|' = \sup_{\|v\|=1} |\langle \phi, v \rangle|$ . Let  $\mathcal{K} \subset \mathcal{V}$  be a nonempty, closed, and convex subset, the *constraint set*; elements of  $\mathcal{K}$  are said to be *admissible*. For a continuous, but generally nonlinear, operator  $f : \mathcal{K} \rightarrow \mathcal{V}'$  and a linear *source functional*  $\ell \in \mathcal{V}'$  we consider the following *variational inequality* (VI) problem: find  $u^* \in \mathcal{K}$  such that

$$(2.1) \quad \langle f(u^*), v - u^* \rangle \geq \langle \ell, v - u^* \rangle \quad \text{for all } v \in \mathcal{K}.$$

Because  $f$  is (generally) nonlinear, the source term  $\ell$  is not strictly needed in stating this class of problems—by redefining  $f$  we may take  $\ell = 0$ —but introducing  $\ell$  will help to clarify later algorithms.

VI (2.1) generalizes nonlinear systems of equations (i.e.  $f(u^*) = \ell$ ) to cases where  $u^*$  is also constrained to be in  $\mathcal{K}$ . Pretending the dual pairing is an inner product, (2.1) says that the angle between  $f(u^*) - \ell$  and any arbitrary vector  $v - u^*$  pointing from  $u^*$  into  $\mathcal{K}$  is at most  $90^\circ$ ; if  $u^*$  solves (2.1) then the dual vector  $f(u^*) - \ell$  points straight into  $\mathcal{K}$ . If  $u^*$  is in the interior of  $\mathcal{K}$  then (2.1) implies  $f(u^*) = \ell$ . Note that variational inequalities generally permit multiple solutions [20].

The following definitions are standard [29, for example].

**DEFINITION 2.1.** *An operator  $f : \mathcal{K} \rightarrow \mathcal{V}'$  is monotone if*

$$(2.2) \quad \langle f(u) - f(v), u - v \rangle \geq 0 \quad \text{for all } u, v \in \mathcal{K},$$

*strictly monotone if equality in (2.2) implies  $u = v$ , and coercive if there exists  $w \in \mathcal{K}$  so that*

$$(2.3) \quad \frac{\langle f(u) - f(w), u - w \rangle}{\|u - w\|} \rightarrow +\infty \quad \text{as } \|u\| \rightarrow +\infty.$$

It is well-known that if  $f : \mathcal{K} \rightarrow \mathcal{V}'$  is continuous, monotone, and coercive then VI (2.1) has a solution [29, Corollary III.1.8], and that the solution is unique when  $f$  is strictly monotone. As in the calculus of variations, coercivity permits a compactness argument for unbounded sets  $\mathcal{K}$  using the fact that closed and bounded subsets of a reflexive Banach space are weakly compact.

Some operators considered below satisfy a stronger inequality than (2.3).

DEFINITION 2.2. Let  $p > 1$ . The operator  $f : \mathcal{K} \rightarrow \mathcal{V}'$  is  $p$ -coercive if there exists  $\kappa > 0$  such that

$$(2.4) \quad \langle f(u) - f(v), u - v \rangle \geq \kappa \|u - v\|^p \quad \text{for all } u, v \in \mathcal{K}.$$

It is easy to see that if  $f$  is  $p$ -coercive then it is monotone, strictly monotone, and coercive. Thus if  $f : \mathcal{K} \rightarrow \mathcal{V}'$  is continuous and  $p$ -coercive ( $p > 1$ ) then there exists a unique  $u^* \in \mathcal{K}$  solving VI (2.1).

Let  $\Omega \subset \mathbb{R}^d$  denote a bounded, open set with piecewise-smooth boundary. Sobolev spaces [18] will be denoted by  $W^{k,p}(\Omega)$ , for integer  $k$  and  $1 \leq p \leq \infty$ , with  $W_0^{1,p}(\Omega)$  denoting the subspace with zero trace along  $\partial\Omega$ . The following example includes the classical and  $p$ -Laplacian obstacle problems [14].

Example 2.3. Let  $1 < p < \infty$ . For  $u, v \in \mathcal{V} = W_0^{1,p}(\Omega)$ , define  $f : \mathcal{V} \rightarrow \mathcal{V}'$  by

$$(2.5) \quad \langle f(u), v \rangle = \int_{\Omega} |\nabla u|^{p-2} \nabla u \cdot \nabla v \, dx.$$

It follows from inequalities for  $|\cdot|^p$  in  $\mathbb{R}^d$ , and the Poincaré inequality, that  $f$  is  $p$ -coercive [14]; see also [10, Appendix A].

Note that for monotone operators VI (2.1) also generalizes the problem of minimizing a convex function over  $\mathcal{K}$ . Suppose  $F : \mathcal{K} \rightarrow \mathbb{R}$  is lower semi-continuous and (Gâteaux) differentiable with continuous derivative  $F' : \mathcal{K} \rightarrow \mathcal{V}'$ . Then  $F$  is convex if and only if  $f = F'$  is monotone, in which case (2.1) holds if and only if

$$(2.6) \quad u^* = \arg \min_{v \in \mathcal{K}} F(v) - \langle \ell, v \rangle.$$

(See e.g. Propositions I.5.5 and II.2.1 in [16] for these facts.) The CD methods of Tai [32] address problem (2.6); his analysis supposes that an objective  $F$  exists with  $F'$  2-coercive. In Example 2.3

$$(2.7) \quad F(v) = \frac{1}{p} \int_{\Omega} |\nabla v|^p \, dx$$

is a convex functional and  $F' = f$  is given by (2.5).

Next we give two examples which are *not* of optimization type (2.6). The first is an advection-diffusion problem; it requires the following Lemma.

LEMMA 2.4. [17] Suppose  $\mathbf{X} : \Omega \rightarrow \mathbb{R}^d$  is a bounded and boundedly-differentiable vector field on  $\Omega$  with  $\nabla \cdot \mathbf{X} = 0$ . For  $u, v \in W^{1,2}(\Omega)$  let  $b(u, v) = \int_{\Omega} (\mathbf{X} \cdot \nabla u) v \, dx$ . Then  $b(u, u) = \frac{1}{2} \int_{\partial\Omega} u^2 \mathbf{X} \cdot \mathbf{n} \, dx$  where  $\mathbf{n}$  is the outward normal on  $\partial\Omega$ .

*Proof.* Integration by parts gives  $b(u, v) = -b(v, u) + \int_{\partial\Omega} uv \mathbf{X} \cdot \mathbf{n} \, dx$ .  $\square$

Example 2.5. Suppose  $\partial\Omega$  is partitioned into Dirichlet and Neumann portions,  $\partial\Omega = \partial_D\Omega \cup \partial_N\Omega$ , with  $\partial_D\Omega$  of positive Hausdorff measure. Let  $\mathcal{V} \subset W^{1,2}(\Omega)$  be the space of functions which have zero trace on  $\partial_D\Omega$ . Consider a velocity field  $\mathbf{X}$  on  $\Omega$  satisfying the conditions of Lemma 2.4, and also assume that the flow is outward on the Neumann boundary:  $\mathbf{X} \cdot \mathbf{n} \geq 0$  on  $\partial_N\Omega$ . For  $u, v \in \mathcal{V}$ ,  $\epsilon > 0$ , and  $\phi \in \mathcal{V}'$ , define

$$(2.8) \quad \langle f(u), v \rangle = \epsilon (\nabla u, \nabla v)_{L^2(\Omega)} + b(u, v) - \langle \phi, v \rangle.$$

With this operator, consider VI (2.1) with  $\ell = 0$  for any closed and convex  $\mathcal{K} \subset \mathcal{V}$ . The interior condition [29] of (2.1) is the following linear advection-diffusion equation:

$$(2.9) \quad -\epsilon \nabla^2 u + \mathbf{X} \cdot \nabla u = \phi.$$

On the other hand, it is easy to see that  $|\langle f(u), v \rangle| \leq ((\epsilon + \|\mathbf{X}\|_\infty)\|u\| + \|\phi'\|)\|v\|$ , so  $f : \mathcal{K} \rightarrow \mathcal{V}'$  is continuous. Lemma 2.4 says that the bilinear form  $b(u, v)$  is skew-symmetric up to a term which is nonnegative by the outward flow assumption. From the Poincaré inequality,

$$\begin{aligned} \langle f(u) - f(v), u - v \rangle &= \epsilon \int_{\Omega} |\nabla u - \nabla v|^2 dx + b(u - v, u - v) \\ &= \epsilon \int_{\Omega} |\nabla u - \nabla v|^2 dx + \frac{1}{2} \int_{\partial_N \Omega} (u - v)^2 \mathbf{X} \cdot \mathbf{n} \geq \epsilon C \|u - v\|^2. \end{aligned}$$

Thus  $f$  is 2-coercive and the associated VI problem is well-posed. If  $\mathbf{X} \neq 0$  then  $f \neq F'$  for any objective  $F$ , because  $\langle f(u), v \rangle$  does not possess the symmetry of a gradient: for  $u, v$  which are zero on  $\partial\Omega$ , note that  $\langle f(u), v \rangle - \langle f(v), u \rangle = -2b(u, v)$ .

References [10, 13] consider similar advection-diffusion VI problems to Example 2.5, over  $\mathcal{K} = \{v \geq 0\}$ .

The next VI example is a model for steady ice sheet geometry in a given climate. It is fully nonlinear and not of optimization type. Related VI problems arise for any fluid layer subject to local surface processes which can remove fluid mass [10].

*Example 2.6.* Let  $\Omega \subset \mathbb{R}^2$  be a fixed region of land, and suppose  $b \in C^1(\Omega)$  is the bedrock elevation on  $\Omega$ . Let  $a \in L^2(\Omega)$  denote a given “surface mass balance” function, the annually-averaged rate of ice accumulation (snow) minus melt and runoff. Then the surface elevation  $s \in C(\Omega)$  of a steady-state, isothermal, and non-sliding ice sheet (glacier) under the *shallow ice approximation* (SIA) [24] satisfies the following VI problem: find  $s \in \mathcal{K} = \{s \geq b\}$  such that

$$(2.10) \quad \int_{\Omega} \Gamma(s - b)^{n+2} |\nabla s|^{n-1} \nabla s \cdot \nabla(v - s) dx \geq \int_{\Omega} a(v - s) dx \quad \text{for all } v \in \mathcal{K}.$$

Here  $n > 1$  and  $\Gamma > 0$  are physical constants for ice;  $n = 3$  is a typical exponent [24]. The doubly-nonlinear and doubly-degenerate operator here is

$$(2.11) \quad \langle f(s), v \rangle = \int_{\Omega} \Gamma(s - b)^{n+2} |\nabla s|^{n-1} \nabla s \cdot \nabla v dx.$$

If the bed is flat ( $b = 0$ ) then a power transformation converts (2.11) into form (2.5) with  $p = n + 1$ . Less is understood for general smooth beds  $b$ , but existence holds for (2.10) [26], and a power of a solution will live in a Sobolev space:  $(s - b)^{2p/(p-1)} \in W^{1,p}(\Omega)$ . This theory, and also observations of ice sheets, shows that  $|\nabla s|$  is often unbounded as one approaches the free boundary from the icy ( $s > b$ ) side.

The numerical results in Section 8 come from applying FASCD Algorithms 6.1 and 7.1 to the above Examples.

**3. Constraint decomposition (CD).** Suppose that there are  $m < \infty$  closed linear subspaces  $\mathcal{V}_i \subset \mathcal{V}$ , so that the sum

$$(3.1) \quad \mathcal{V} = \sum_{i=0}^{m-1} \mathcal{V}_i$$

holds in the sense that if  $w \in \mathcal{V}$  then there exist  $w_i \in \mathcal{V}_i$  so that  $w = \sum_i w_i$ . We say (3.1) is a *space decomposition* of  $\mathcal{V}$  [36]. For a closed, convex subset  $\mathcal{K} \subset \mathcal{V}$ , suppose

208 that  $\mathcal{K}_i \subset \mathcal{V}_i$  are nonempty, closed, and convex subsets such that

209 (3.2) 
$$\mathcal{K} = \sum_{i=0}^{m-1} \mathcal{K}_i.$$

210 The sum in (3.2) must hold in two senses [33]: (i) if  $w \in \mathcal{K}$  then there exist  $w_i \in \mathcal{K}_i$   
 211 so that  $w = \sum_i w_i$ , and (ii) if  $z_i \in \mathcal{K}_i$  for each  $i$  then  $\sum_i z_i \in \mathcal{K}$ . Note that neither  
 212 decomposition (3.1) or (3.2) is required to be unique, and also notice that sense (ii) is  
 213 automatic for (3.1) because the  $\mathcal{V}_i$  are subspaces. Finally, suppose there are bounded,  
 214 generally nonlinear, *decomposition operators*  $\Pi_i : \mathcal{K} \rightarrow \mathcal{K}_i$  such that if  $v \in \mathcal{K}$  then

215 (3.3) 
$$v = \sum_{i=0}^{m-1} \Pi_i v,$$

216 with the decomposition operators satisfying the stability property

217 (3.4) 
$$\left( \sum_{i=0}^{m-1} \|\Pi_i u - \Pi_i v\|^2 \right)^{1/2} \lesssim \|u - v\|.$$

218 Clearly (3.3) implies sense (i) for (3.2). A *constraint decomposition* (CD) of  $\mathcal{K}$  is a  
 219 choice of  $\mathcal{V}_i, \mathcal{K}_i, \Pi_i$  satisfying (3.1)–(3.4) [32]. Figure 1 suggests how a low-dimensional  
 220 example might look; note  $\mathcal{K}_i \not\subset \mathcal{K}$  in this and most other cases.

FIG. 1. A *constraint decomposition* (CD) for a unilateral obstacle problem on a two-point space  $\Omega = \{x_1, x_2\}$ , with  $\mathcal{V} = \{v : \Omega \rightarrow \mathbb{R}\}$  and  $\mathcal{K} = \{v \geq \psi\}$ .

221 We will construct a finite-dimensional multilevel CD in Sections 4–7. However, the  
 222 CD concept can also be applied at the level of the continuum problem. For example,  
 223 in a unilateral obstacle problem ( $\mathcal{K} = \{v \geq \psi\}$ ) one can construct an overlapping  
 224 domain decomposition of  $\mathcal{V}$  by using a smooth, finite partition of unity  $\{\varphi_i\}$ , subspaces  
 225  $\mathcal{V}_i = \{w \in \mathcal{V} : w = 0 \text{ if } \varphi_i = 0\}$ , constraint sets  $\mathcal{K}_i = \{v \in \mathcal{V}_i : v \geq \varphi_i \psi\}$ , and  
 226 decomposition operators  $\Pi_i(v) = \varphi_i v$ . More relevant to the current effort, one may  
 227 also construct a CD via a disjoint frequency decomposition of a Hilbert space of  
 228 periodic functions on a cube  $\Omega = (0, 1)^d$ . Reflecting the underlying multigrid idea  
 229 [34], the finite-dimensional FE CD in Section 5, will, in a vague sense, approximate  
 230 such a frequency decomposition.

231 Associated to any CD are certain iterative methods [32, 36]. The following multi-  
 232 plicative/successive CD-MULT algorithm, which generalizes the Gauss–Seidel iteration,  
 233 replaces  $u \in \mathcal{K}$  with a new iterate  $w \in \mathcal{K}$  which should be closer to  $u^* \in \mathcal{K}$  solving

(2.1). Each solution of the “smaller” VI problem over  $\mathcal{K}_i$  corrects the global iterate immediately, and thus the ordering of  $\{\mathcal{K}_i\}$  affects the rate of convergence.

CD-MULT( $u$ ):  
  **for**  $i = 0, \dots, m - 1$ :  
    find  $w_i \in \mathcal{K}_i$  such that  
       $\left\langle f\left(\sum_{j < i} w_j + w_i + \sum_{j > i} \Pi_j u\right), v_i - w_i \right\rangle \geq \langle \ell, v_i - w_i \rangle$  for all  $v_i \in \mathcal{K}_i$   
  **return**  $w = \sum_i w_i \in \mathcal{K}$

The sum “ $\sum_{j > i} \Pi_j u$ ” should be read as “portions of  $u$  needing improvement”. Tai [32] also proposes an additive/parallel version of the algorithm, but it is not used here.

The VI problems inside CD-MULT reduce to constrained line searches when the  $\mathcal{V}_i$  are one-dimensional. If  $e_i = w_i - \Pi_i u \in \mathcal{V}_i$  denotes the correction from  $\mathcal{K}_i$ , then the new iterate  $w = u + \sum_i e_i$  is computed by adding a correction from each subspace  $\mathcal{V}_i$ , but so that  $w \in \mathcal{K}$ ; the corrections preserve admissibility.

If VI problem (2.1) corresponds to convex optimization (2.6) then CD-MULT generates monotonically-decreasing objective values.

LEMMA 3.1. [32] Suppose  $f = F'$  for  $F : \mathcal{K} \rightarrow \mathbb{R}$  convex and differentiable, and let  $u \in \mathcal{K}$ . The output  $w \in \mathcal{K}$  from CD-MULT satisfies

$$(3.5) \quad F(w) - \langle \ell, w \rangle \leq F(u) - \langle \ell, u \rangle.$$

However, CD-MULT is meaningful whether or not we are in the optimization case  $f = F'$ , and even if  $f$  is nonlinear, non-local, or defined only on  $\mathcal{K}$ . Practical and efficient FE implementation for such general operators  $f$  seems not to have been addressed in the literature. In particular, references [23, 32] only apply the multilevel CD method to the classical obstacle problem, wherein  $f = F'$  is linear, local, and defined on all of  $\mathcal{V}$ . In Section 6 we will extend multilevel CD iterations to general nonlinear operators by applying the full approximation scheme (FAS) idea of Brandt [5], and then illustrate its application to general operators in Section 8.

From now on we restrict to the case of *box constraints* [3, 22], also called bilateral obstacle problems, over  $\mathcal{V} = W^{1,p}(\Omega)$ . The *lower obstacle*  $\underline{\gamma}$  and *upper obstacle*  $\bar{\gamma}$  are given measurable functions, defined on the closure  $\bar{\Omega}$ , with values in the extended real line  $\mathbb{R} = [-\infty, +\infty]$ , satisfying the following properties:  $\underline{\gamma} < +\infty$ ,  $\bar{\gamma} > -\infty$ , and  $\underline{\gamma} \leq \bar{\gamma}$ . We also suppose that  $\partial\Omega$  is split into disjoint sets  $\partial\bar{\Omega} = \partial_D\Omega \cup \partial_N\Omega$ , with  $\partial_D\Omega$  of positive Hausdorff measure, and  $\partial_N\Omega$  possibly empty. Dirichlet data is given by  $g_D : \partial_D\Omega \rightarrow \mathbb{R}$ , and we assume  $\underline{\gamma} \leq g_D \leq \bar{\gamma}$  on  $\partial_D\Omega$ . Now define

$$(3.6) \quad \mathcal{K} = \left\{ w : \underline{\gamma} \leq w \leq \bar{\gamma} \text{ and } w|_{\partial_D\Omega} = g_D \right\} \subset \mathcal{V} = W^{1,p}(\Omega),$$

the closed and convex *constraint set*. (Observe that this treats inequality constraints and Dirichlet conditions in a unified manner.) Dirichlet values are in the trace sense [18], and  $g_D$  is assumed to be as regular as needed. Any Neumann conditions over  $\partial_N\Omega$  are imposed weakly by the operator  $f$ , via an integral over  $\partial_N\Omega$ .

**4. Multilevel finite elements.** We will approximate solutions of box-constrained VI problems (2.1), (3.6) using finite elements (FE). In this Section a nested, multilevel, and  $P_1$  or  $Q_1$  element [17] mesh hierarchy is constructed by refinement of a coarse

mesh. This hierarchy permits the construction of a multilevel CD of the finest-level constraint set in Section 5.

The construction is by standard nested refinement as follows. Let  $\Omega \subset \mathbb{R}^d$  be an open bounded polygon and suppose  $\mathcal{T}^0$  is the *coarsest mesh*, a finite set of non-overlapping, nondegenerate cells with union equal to  $\overline{\Omega}$  and maximum cell diameter (mesh size)  $h_0 > 0$ . We assume  $\mathcal{T}^0$  is conforming, with no hanging nodes. For  $j = 1, \dots, J$ , let  $\mathcal{T}^j$  be the uniform refinement of  $\mathcal{T}^{j-1}$ ; each  $\mathcal{T}^{j-1}$  cell becomes  $2^d$  cells in  $\mathcal{T}^j$  with mesh size  $h_j = 2^{-j}h_0$ . We call  $\mathcal{T}^J$  the *finest-level mesh* and  $J + 1$  the *number of levels*. Let  $m_j$  be the number of vertices in  $\mathcal{T}^j$ , the number of degrees of freedom at the  $j$ th level.

As is common in the discretization of variational inequalities, we employ lowest-order continuous Lagrange elements  $P_1$  or  $Q_1$  on simplices and tensor-product cells respectively.<sup>1</sup> Let  $\mathcal{V}^j$  be such nested FE spaces over each mesh  $\mathcal{T}^j$ , with arbitrary boundary values:

$$(4.1) \quad \mathcal{V}^0 \subset \mathcal{V}^1 \subset \dots \subset \mathcal{V}^J \subset \mathcal{V} = W^{1,p}(\Omega).$$

The choice of  $P_1$  or  $Q_1$  is convenient because it enjoys *nodal monotonicity*:

$$(4.2) \quad \mathbf{w} \geq \mathbf{z} \implies w \geq z$$

for all  $w, z \in \mathcal{V}^j$ , where  $\mathbf{w}, \mathbf{z} \in \mathbb{R}^{m_j}$  denote vectors of nodal values. In other words, to enforce an inequality constraint over  $\mathcal{V}^j$  we need only enforce it pointwise on the degrees of freedom. By contrast, for  $k \geq 2$  there are functions in the standard bases of  $P_k$  and  $Q_k$  which take on negative values [17, Figure 1.7], violating (4.2).

To construct box constraints on all meshes in the hierarchy, let  $\tilde{\mathcal{V}}^j$  denote the set of  $\tilde{\mathbb{R}} = [-\infty, +\infty]$  valued functions on the vertices of  $\mathcal{T}^j$ . The finest-level *lower* and *upper obstacles*  $\underline{\gamma}^J, \bar{\gamma}^J \in \tilde{\mathcal{V}}^J$  are constructed by suitable interpolation of  $\underline{\gamma}, \bar{\gamma}$ , e.g. by applying the Cl  ment interpolation operator [12]. These obstacles must satisfy  $\underline{\gamma}^J < +\infty$ ,  $-\infty < \bar{\gamma}^J$ , and  $\underline{\gamma}^J \leq \bar{\gamma}^J$ . On the finest-level mesh the discrete boundary data  $g_D^J \in \mathcal{V}^J$  is assumed to satisfy  $g_D^J = g_D$  on  $\partial_D \Omega$ —this restricts  $g_D$  in (3.6) to be piecewise-linear—and  $\underline{\gamma}^J \leq g_D^J \leq \bar{\gamma}^J$  at those vertices of  $\mathcal{T}^J$  which lie in  $\partial_D \Omega$ . Then we define

$$(4.3) \quad \mathcal{K}^J = \{w : \underline{\gamma}^J \leq w \leq \bar{\gamma}^J \text{ on vertices of } \mathcal{T}^J, \text{ and } w|_{\partial_D \Omega} = g_D^J|_{\partial_D \Omega}\} \subset \mathcal{V}^J.$$

This nonempty, closed, and convex subset is the finest-level *constraint set*.

Let  $f^J : \mathcal{K}^J \rightarrow (\mathcal{V}^J)'$  be a discretization of  $f$  in (2.1). Note that, by inclusion (4.1),  $\ell^J = \ell$  is defined and continuous over  $\mathcal{V}^J$ . We seek the FE solution  $u^J \in \mathcal{K}^J$  of the finest-level, finite-dimensional, nonlinear VI:

$$(4.4) \quad \langle f^J(u^J), v - u^J \rangle \geq \langle \ell^J, v - u^J \rangle \quad \text{for all } v \in \mathcal{K}^J.$$

If  $f^J$  is continuous and  $p$ -coercive on  $\mathcal{K}^J$  then (4.4) is well-posed.

While (4.4) approximates (2.1), we warn the reader that it is usually not a conforming FE method. That is, even if quadrature and other implementation details for  $f^J$  are ignored, and despite the vector space inclusion  $\mathcal{V}^J \subset \mathcal{V}$ , from definitions (3.6) and (4.3) we do not expect  $\mathcal{K}^J \subset \mathcal{K}$  in general [15, section 5.1]. Even for continuous obstacles  $\underline{\gamma}, \bar{\gamma}$ , FE admissibility (4.3) will generally not imply  $\mathcal{K}$ -admissibility (3.6).

<sup>1</sup>Keith & Surowiec have recently proposed a scheme for solving VIs using high-order finite elements [28].



For a practical consequence of this situation, regarding Example 2.6, nodal bed elevation data in a glacier application will miss the topographic detail between the nodes [9].

The multilevel algorithm of Section 6 requires five transfer operators between meshes, and Table 1 will help the reader keep track. Three of these are already employed in standard FAS [34], and they are linear maps defined as follows. First, canonical prolongation  $P : \mathcal{V}^{j-1} \rightarrow \mathcal{V}^j$  implements the vector space inclusion (4.1). Second, canonical (dual) restriction  $R : (\mathcal{V}^j)' \rightarrow (\mathcal{V}^{j-1})'$  is defined for  $\sigma \in (\mathcal{V}^j)'$  as  $\langle R\sigma, z \rangle = \langle \sigma, z \rangle$  for all  $z \in \mathcal{V}^{j-1} \subset \mathcal{V}^j$ . (These canonical transfers imply a change of FE representation;  $R$  is “full-weighting” [34].) Finally, to define injection  $R^\bullet : \mathcal{V}^j \rightarrow \mathcal{V}^{j-1}$ , note that the vertices of  $\mathcal{T}^{j-1}$  are vertices of  $\mathcal{T}^j$ . Thus for  $z \in \mathcal{V}^j$  we define  $R^\bullet z$  as the element of  $\mathcal{V}^{j-1}$  with the same (coarse) nodal values. Injection is monotonic in the sense that if  $w \leq z$  then  $R^\bullet w \leq R^\bullet z$ .

<i>name</i>	<i>mapping</i>	<i>linear?</i>
canonical prolongation	$P : \mathcal{V}^{j-1} \rightarrow \mathcal{V}^j$	✓
canonical (dual) restriction	$R : (\mathcal{V}^j)' \rightarrow (\mathcal{V}^{j-1})'$	✓
(nodal) injection	$R^\bullet : \mathcal{V}^j \rightarrow \mathcal{V}^{j-1}$	✓
maximum injection	$R^\oplus : \tilde{\mathcal{V}}^j \rightarrow \tilde{\mathcal{V}}^{j-1}$	✗
minimum injection	$R^\ominus : \tilde{\mathcal{V}}^j \rightarrow \tilde{\mathcal{V}}^{j-1}$	✗

TABLE 1  
Transfer operators used in this paper.

The monotone injections  $R^\oplus, R^\ominus$  [32, 23] in Table 1 will only be applied to constraints in the  $\mathbb{R}$ -valued nodal spaces  $\mathcal{V}^j$ . They are nonlinear maps which maximize and minimize, respectively, nodal values over the open supports of coarser-mesh basis functions (i.e. over the stars of the coarse vertices). To make the construction precise, let  $x_q^j$  denote a vertex of mesh  $\mathcal{T}^j$ , with corresponding basis function  $\psi_q^j$ . For  $z \in \mathcal{V}^j$  we define new functions in  $\tilde{\mathcal{V}}^{j-1}$ :

$$(4.5) \quad \begin{aligned} (R^\oplus z)(x_p^{j-1}) &= \max\{z(x_q^j) : \psi_p^{j-1}(x_q^j) > 0\}, \\ (R^\ominus z)(x_p^{j-1}) &= \min\{z(x_q^j) : \psi_p^{j-1}(x_q^j) > 0\}. \end{aligned}$$

These operators are constructed to imply

$$(4.6) \quad R^\ominus z \leq z \leq R^\oplus z.$$

An illustration of the construction is given in Figure 2. Implementing these operators on non-nested meshes could be done efficiently using a supermesh [21]. In the next Section we will use  $R^\oplus, R^\ominus$  to construct “level defect constraints” such that the zero function is always admissible, a construction which depends on these additional ordering properties which follow from (4.5):

$$(4.7) \quad z \geq 0 \implies R^\ominus z \geq 0 \quad \text{and} \quad z \leq 0 \implies R^\oplus z \leq 0.$$

**5. Multilevel CDs via level defect constraints.** A key choice in devising a multilevel scheme for VIs is in the construction of bounds for the coarser levels. Our multilevel CD scheme uses *defect constraints* [23] derived from an admissible finest-level iterate. The next Example illustrates why we do *not*, with the exception of

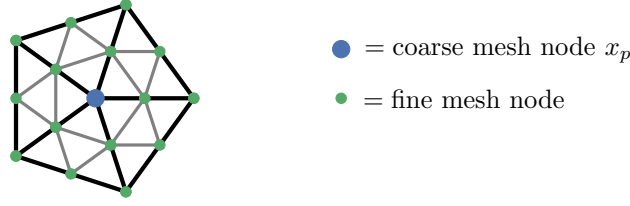


FIG. 2. The monotone injection operators  $R^\oplus$  and  $R^\ominus$  assign to a coarse degree of freedom (blue) the maximum and minimum respectively of the fine function over the patch of coarse cells sharing its vertex. The coarse mesh is in black and the fine in grey.

an interpolation needed for the FMG method of Section 7, apply injection operators directly to the finest-level box constraints  $\underline{\gamma}^J, \bar{\gamma}^J$ .

*Example 5.1.* Let  $\Omega = (0, L) \subset \mathbb{R}^1$  and consider a two-level mesh hierarchy ( $J = 1$ ). Let  $\underline{\gamma}^1$  be a sawtooth function with minimum value zero, and suppose  $\bar{\gamma}^1 = C + \underline{\gamma}^1$  with  $C > 0$  strictly less than the maximum of  $\underline{\gamma}^1$ . Figure 3 shows such functions on  $\bar{\mathcal{T}}^1$  with five vertices. For appropriate boundary conditions the fine-level constraint set  $\mathcal{K}^1$  defined by (4.3) is nonempty. However, various schemes to coarsen the constraints by direct transfers of  $\underline{\gamma}^1, \bar{\gamma}^1$  are doomed to failure. Suppose

$$(5.1) \quad \underline{\gamma}^0, \bar{\gamma}^0 \equiv R^\bullet \underline{\gamma}^1, R^\bullet \bar{\gamma}^1. \quad [\text{problematic}]$$

Then  $\underline{\gamma}^0 = 0$  and  $\bar{\gamma}^0 = C$  identically. In that case the corresponding constraint set  $\mathcal{K}^0$  is nonempty, but prolongation  $Pw^0$  of an admissible solution of the coarse problem ( $w^0 \in \mathcal{K}^0$ ;  $\underline{\gamma}^0 \leq w^0 \leq \bar{\gamma}^0$ ) is never admissible on the finer level ( $Pw^0 \notin \mathcal{K}^1$ ). Attempting to fix this by projecting (truncating) into  $\mathcal{K}^1$  would introduce high frequencies not present in  $w^0$ . On the other hand, if

$$(5.2) \quad \underline{\gamma}^0, \bar{\gamma}^0 \equiv R^\oplus \underline{\gamma}^1, R^\ominus \bar{\gamma}^1 \quad [\text{problematic}]$$

then the coarse-level constraint set  $\mathcal{K}^0$  is empty because  $\underline{\gamma}^0 > \bar{\gamma}^0$  (Figure 3, right).

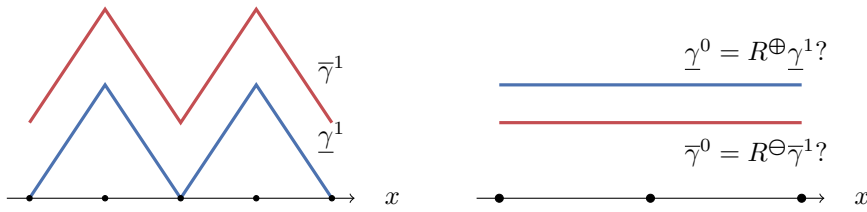


FIG. 3. For the finer-level constraints  $\underline{\gamma}^1$  (blue) and  $\bar{\gamma}^1$  (red) on the left, direct application of  $R^\bullet, R^\ominus, R^\oplus$  to generate coarser-level constraints is problematic. Possibility (5.2), which generates an empty coarser-level set  $\mathcal{K}^0$ , is at right. Defect constraints (5.3) avoid such difficulties.

However, we can construct iterate-dependent constraints which satisfy ordering (5.5) below, and which bypass the difficulties in the above Example. Suppose  $w^J \in \mathcal{K}^J$  is an admissible iterate; see (4.3). We define the *finest-level defect constraints* [23] as functions in  $\tilde{\mathcal{V}}^J$ :

$$(5.3) \quad \underline{\chi}^J = \underline{\gamma}^J - w^J, \quad \bar{\chi}^J = \bar{\gamma}^J - w^J.$$

(If  $\underline{\gamma}^J = -\infty$  then  $\underline{\chi}^J = -\infty$  by definition, and similarly if  $\bar{\gamma}^J = +\infty$  then  $\bar{\chi}^J = +\infty$ .)  
 Definition (4.3) implies that  $\underline{\chi}^J \leq 0 \leq \bar{\chi}^J$  on  $\bar{\Omega}$ . Observe that a corrected iterate  $w^J + z^J$  is admissible, i.e.  $w^J + z^J \in \mathcal{K}^J$ , if and only if  $z^J \in \mathcal{V}^J$  is zero on  $\partial_D \Omega$  and bounded by the defect constraints,  $\underline{\chi}^J \leq z^J \leq \bar{\chi}^J$ .

To descend to coarser levels,  $j = J-1, \dots, 1, 0$ , we apply the monotone injections to generate *level defect constraints* (LDCs) in  $\tilde{\mathcal{V}}^j$ :<sup>2</sup>

$$(5.4) \quad \underline{\chi}^j = R^\oplus \underline{\chi}^{j+1}, \quad \bar{\chi}^j = R^\ominus \bar{\chi}^{j+1}.$$

Observe that by (4.6) and (4.7),

$$(5.5) \quad \underline{\chi}^J \leq \dots \leq \underline{\chi}^0 \leq 0 \leq \bar{\chi}^0 \leq \dots \leq \bar{\chi}^J.$$

The LDC  $\underline{\chi}^j$  is the most-negative function from  $\tilde{\mathcal{V}}^j$  such that if an element of  $\tilde{\mathcal{V}}^j$  is above  $\underline{\chi}^j$  then it is also above  $\underline{\chi}^{j+1}$ ; corresponding comments apply to  $\bar{\chi}^j$ . Note that for Algorithm 6.1 below, any system satisfying (5.5) will suffice; the particular formulas in (5.4) are not actually required.

This construction of multilevel box constraints, likewise of the unilateral construction in [23], should permit large, yet admissible, coarse corrections, which promotes multilevel solver efficiency. However, when coarsening the problem downward in a V-cycle, we observe that one cannot predict the upcoming coarser corrections and so one must construct constraint sets from which any sum will be admissible. With this in mind, and looking forward to telescoping sums (5.9), we compute the LDC differences [23]:

$$(5.6) \quad \phi^j = \underline{\chi}^j - \underline{\chi}^{j-1}, \quad \bar{\phi}^j = \bar{\chi}^j - \bar{\chi}^{j-1}.$$

(Take  $\underline{\chi}^{-1} = \bar{\chi}^{-1} = 0$  so that  $\phi^0 = \underline{\chi}^0$  and  $\bar{\phi}^0 = \bar{\chi}^0$ . By definition, if  $\underline{\chi}^j(x_p) = -\infty$  then we set  $\phi^j(x_p) = -\infty$  regardless of the value of  $\underline{\chi}^{j-1}(x_p)$ , and etc.) Note that while  $\phi^j, \bar{\phi}^j \in \tilde{\mathcal{V}}^j$  do bracket zero, they are not ordered as in (5.5).

Now we define *downward* and *upward constraint sets*, respectively, as certain closed and convex subsets of the FE spaces  $\mathcal{V}^j$ :

$$(5.7) \quad \mathcal{D}^j = \left\{ v \in \mathcal{V}^j : \phi^j \leq v \leq \bar{\phi}^j \text{ and } v|_{\partial_D \Omega} = 0 \right\},$$

$$\mathcal{U}^j = \left\{ v \in \mathcal{V}^j : \underline{\chi}^j \leq v \leq \bar{\chi}^j \text{ and } v|_{\partial_D \Omega} = 0 \right\}.$$

Because  $\underline{\chi}^j \leq \phi^j \leq 0 \leq \bar{\phi}^j \leq \bar{\chi}^j$ , it follows that  $\mathcal{D}^j \subseteq \mathcal{U}^j$ . Note that the finest-level upward set  $\mathcal{U}^J$  is equivalent to the original constraint set  $\mathcal{K}^J$ : for all  $z^J \in \mathcal{V}^J$ ,  $z^J \in \mathcal{U}^J$  if and only if  $w^J + z^J \in \mathcal{K}^J$ .

The V-cycle solver in the next Section (Algorithm 6.1) will compute corrections from  $\mathcal{D}^j$  and  $\mathcal{U}^j$ . For general box constraints the upward direction is, however, based on *incomplete* CDs as we now explain. Each upward set  $\mathcal{U}^j$  is generally only a superset of a sum of downward sets  $\mathcal{D}^j$ , though this becomes a true CD satisfying (3.1)–(3.4) in unilateral cases. The following Lemma, apparently new, extends the unilateral CD construction underlying Algorithm 4.2 in [23]; see also equation (59) in [32].

LEMMA 5.2.

$$(5.8) \quad \mathcal{U}^j \supseteq \mathcal{D}^j + \mathcal{D}^{j-1} + \dots + \mathcal{D}^0$$

<sup>2</sup>The definition of  $\underline{\chi}^j$  matches that in Section 4 of [23]; see (4.22) and Figure 4.1 therein.

for  $j = 0, 1, \dots, J$ . In unilateral cases, where either  $\underline{\gamma}^J = -\infty$  or  $\overline{\gamma}^J = +\infty$  identically, inclusion (5.8) becomes a full CD with  $\mathcal{U}^j = \sum_{i=0}^j \mathcal{D}^i$ .

*Proof.* From nesting (4.1), subspace decomposition (3.1) holds, and definition (5.7) shows  $\mathcal{D}^i \subset \mathcal{U}^i \subset \mathcal{V}^i$ . Furthermore, telescoping sums hold for any  $j = 0, 1, \dots, J$ :

$$(5.9) \quad \sum_{i=0}^j \underline{\phi}^i = \underline{\chi}^j, \quad \sum_{i=0}^j \overline{\phi}^i = \overline{\chi}^j.$$

Thus if  $y^i \in \mathcal{D}^i$  for  $0 \leq i \leq j$  then

$$(5.10) \quad \underline{\chi}^j = \sum_{i=0}^j \underline{\phi}^i \leq \sum_{i=0}^j y^i \leq \sum_{i=0}^j \overline{\phi}^i \leq \overline{\chi}^j,$$

so (5.8) holds for any box constraints.

In unilateral cases we can also construct decomposition operators  $\Pi_i$  and thereby show (3.3). For concreteness suppose  $\overline{\gamma}^J = +\infty$ , thus  $\overline{\chi}^j = +\infty$  and  $\overline{\phi}^i = +\infty$  for all levels; the  $\underline{\gamma}^J = -\infty$  case is similar. For  $v \in \mathcal{V}^j$  and  $0 \leq i \leq j$ , let  $I_{j \rightarrow i}^\ominus : \tilde{\mathcal{V}}^j \rightarrow \tilde{\mathcal{V}}^i$  be the operator applying the minimum (monotone) injection  $j - i$  times:  $I_{j \rightarrow i}^\ominus v = R^\ominus(\dots(R^\ominus v)\dots)$ . (Set  $I_{j \rightarrow j}^\ominus v = v$  and  $I_{j \rightarrow -1}^\ominus = 0$  by definition.) Now define nonlinear decomposition operators  $\Pi_i : \mathcal{U}^j \rightarrow \mathcal{D}^i$ :

$$(5.11) \quad \Pi_i z^j := I_{j \rightarrow i}^\ominus(z^j - \underline{\chi}^j) - I_{j \rightarrow i-1}^\ominus(z^j - \underline{\chi}^j) + \underline{\phi}^i.$$

(Compare equation (4.9) in [23].) Property (4.6) implies  $I_{j \rightarrow i}^\ominus(z^j - \underline{\chi}^j) \geq I_{j \rightarrow i-1}^\ominus(z^j - \underline{\chi}^j)$ , thus  $\Pi_i z^j \geq \underline{\phi}^i$ , so  $\Pi_i z^j \in \mathcal{D}^i$ , and furthermore stability (3.4) holds [23, Theorem 4.2]. On the other hand, the following sum telescopes, leaving only its first term plus the sum in (5.9):

$$\sum_{i=0}^j \Pi_i z^j = z^j - \underline{\chi}^j + \sum_{i=0}^j \underline{\phi}^i = z^j.$$

This shows (3.3), thus (3.2), and that (5.8) is equality.  $\square$

One might try to convert (5.8) into a full CD for arbitrary box constraints by attempting to construct decomposition maps  $\Pi_i$  as follows. One can split  $z^j = \min\{z^j, 0\} + \max\{z^j, 0\}$  and apply unilateral formulas (5.11) to  $\min\{z^j, 0\}$  and  $\max\{z^j, 0\}$  separately. The above proof shows that the lower bound  $\Pi_i(\min\{z^j, 0\}) \geq \underline{\phi}^i$  does hold. However, the following Example shows why  $\Pi_i(\min\{z^j, 0\})$  may have an arbitrarily large maximum, and thus exceed any finite upper LDC  $\overline{\phi}^i$ . In fact,  $\Pi_i$  defined above does not generally map all non-positive elements of  $\mathcal{U}^J$  into  $\mathcal{D}^i$  in cases where a finite upper LDC is present.

*Example 5.3.* Let  $a > 0$  be an arbitrary positive number. Consider a 2-level hierarchy ( $J = 1$ ), and suppose the lower defect constraint is the constant function  $\underline{\chi}^1 = -a$ . Note  $\underline{\chi}^0 = R^\oplus \underline{\chi}^1 = -a$  also, so  $\underline{\phi}^1 = 0$  and  $\underline{\phi}^0 = -a$ . Suppose  $z^1$  is a “sawtooth” function which takes on value  $-a$  on the coarse vertices and value 0 on the other vertices. Then, for any  $\overline{\chi}^1 \geq 0$ , we have  $\overline{\chi}^1 \geq 0 \geq z^1 \geq \underline{\chi}^1$ , so  $z^1 \in \mathcal{U}^1$ . However,  $I_{1 \rightarrow 0}^\ominus(z^1 - \underline{\chi}^1) = R^\ominus(z^1 - \underline{\chi}^1) = 0$  identically. From (5.11),  $\Pi_1 z^1$  simplifies to  $\Pi_1 z^1 = z^1 - \underline{\chi}^1$ . But then  $\Pi_1 z^1$  attains a maximum  $a \geq 0$ . This maximum can be chosen to exceed any upper defect obstacle  $\overline{\phi}^1$ , and  $\Pi_1 z^1 \notin \mathcal{D}^1$  would then occur.

This Example does not exclude other strategies for showing full CDs in the general box-constrained case.

In any case, each upward set  $\mathcal{U}^j$  can be decomposed, incompletely in the sense of (5.8), down to an arbitrary coarser level. The next Lemma does not follow from Lemma 5.2.

LEMMA 5.4. *For any  $j = 0, 1, \dots, J$  and  $0 \leq k \leq j$ ,*

$$(5.12) \quad \mathcal{U}^j \supseteq \mathcal{D}^j + \mathcal{D}^{j-1} + \dots + \mathcal{D}^{k+1} + \mathcal{U}^k$$

*In unilateral cases, where either  $\underline{\gamma}^J = -\infty$  or  $\bar{\gamma}^J = +\infty$ , it follows that  $\mathcal{U}^j = \mathcal{U}^k + \sum_{i=k+1}^j \mathcal{D}^i$  is a full CD.*

*Proof.* Definition (5.6) shows inclusion (5.12). In unilateral cases we may follow the proof of Lemma 5.2 with (5.11) unchanged for  $i = k+1, \dots, j$ , but modified in the  $i = k$  case:  $\Pi_k z^j = I_{j \rightarrow k}^\ominus(z^j - \underline{\chi}^j) + \underline{\chi}^k$ . Otherwise the proof goes through as before.  $\square$

Inclusions (5.8) and (5.12) imply the admissibility of all iterates and corrections in Algorithm 6.1 below. These inclusions are special to multilevel schemes based on defect constraints, and they hold regardless of whether decomposition operators  $\Pi_i$  can be constructed. We propose a new, incomplete variant of the CD-MULT iteration which requires no operators  $\Pi_i$ . For  $w^J \in \mathcal{K}^J$ , and (input) downward perturbations  $y^i \in \mathcal{D}^i$ , it applies in the special case where inclusion (5.12) holds:

```

ICD-TELE( $w^J, \{y^i\}_{i=1}^J$ ):
  for  $j = 0, \dots, J$ :
    find  $z^j \in \mathcal{U}^j$  so that for all  $v \in \mathcal{U}^j$ ,
       $\left\langle f\left(w^J + \sum_{i>j} y^i + z^j\right), v - z^j \right\rangle \geq \langle \ell, v - z^j \rangle$ 
  return  $\tilde{w}^J = w^J + z^J$ 

```

The downward perturbation  $y^j$ , which apparently disappears as ICD-TELE proceeds, actually helps in constructing an initial iterate for  $z^j$ ; see Algorithm 6.1.

Algorithm 6.1 below incorporates ICD-TELE for up-smoothing in the larger constraint sets  $\mathcal{U}^j$ . The observation that this can be more efficient, illustrated by Example 8.2 in particular, seems to be new. For comparison,  $V(1,1)$  cycles in [23] use half-size versions of the smaller sets  $\mathcal{D}^j$  both on descent and ascent; see also [32, section 5.4]. On the other hand, any convergence analysis extending the arguments of [23, 32] might require full CDs.

**6. FASCD V-cycle.** The V-cycle in this Section extends the multilevel CD schemes of Tai [32] and Gräser & Kornhuber [23, Algorithm 4.2] by following a non-linear full approximation scheme (FAS) approach [7]. Our V-cycle reduces to FAS for PDEs when inequality constraints are removed. Each V-cycle generates a correction to a finest-level iterate  $w^J \in \mathcal{K}^J$ , via information from each coarser FE subspace  $\mathcal{V}^j$ , by approximately solving VI problems in constraint sets  $\mathcal{D}^j$  and  $\mathcal{U}^j$  during the downward and upward stages, respectively. The corrections are constructed so that iterates remain admissible at every level. A key idea is that up-smoothing solves less-restricted VI problems, in larger subsets, than down-smoothing. Going downward one does not know what coarse corrections are coming, thus one must choose the smaller constraint sets ( $\mathcal{D}^j$ ) so the correction sum is admissible once we return to a given

level. Going upward, however, no further coarse corrections can violate admissibility, so we may relax in the larger sets  $\mathcal{U}^j$ .

Suppose that  $y^i \in \mathcal{D}^i$ , for  $i = J, \dots, j+1$ , are already-computed corrections during the downward part of the V-cycle (Figure 4, left). By (5.8) the correction at this point is admissible, namely  $y^J + \dots + y^{j+1} \in \mathcal{U}^J$ , equivalently  $w^J + y^J + \dots + y^{j+1} \in \mathcal{K}^J$ . Relaxation then occurs at the next-coarser level, yielding the next correction  $y^j \in \mathcal{D}^j$ . Solving the coarsest-level VI results in the full downward correction  $y^J + \dots + y^1 + z^0 \in \mathcal{U}^J$ . Starting upward,  $y^1 + z^0 \in \mathcal{U}^1$  is an initial iterate for relaxation on level  $j = 1$ , which then yields  $z^1 \in \mathcal{U}^1$  and an admissible correction  $y^J + \dots + y^2 + z^1 \in \mathcal{U}^J$ , using inclusion (5.12). Continuing in this “telescoping” way by up-smoothing in the constraint sets  $\mathcal{U}^j$ , starting from initial iterate  $y^j + z^{j-1}$ , finally generates  $z^J \in \mathcal{U}^J$  as the V-cycle correction. The new finest-level iterate is  $\tilde{w}^J = w^J + z^J \in \mathcal{K}^J$ .

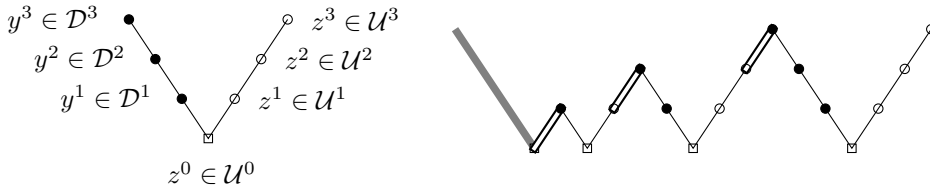


FIG. 4. Left: FASCD V-cycle Algorithm 6.1 computes downward corrections  $y^j \in \mathcal{D}^j$ , but the upward corrections  $z^j \in \mathcal{U}^j$  are in larger sets. Right: FMG Algorithm 7.1 generates initial iterates on finer levels via injection and truncation (doubled edges).

We must specify the problems which are to be solved at each mesh level. As in FAS multigrid for nonlinear PDEs [7, 8, 34], both the solution approximation and the residual must be coarsened, and a source functional created. On any mesh level  $j$  we assume there is a re-discretized nonlinear operator  $f^j$ , with output in  $(\mathcal{V}^j)'$ , which is an FE discretization of  $f$  in (2.1). At the start of each V-cycle we assume that an admissible iterate  $w^J \in \mathcal{K}^J$  has been used to generate the LDCs and constraint sets  $\mathcal{D}^j, \mathcal{U}^j$  at each level (Section 5).

As we descend we define the initial  $j$ th-level iterates

$$(6.1) \quad w^j = R^\bullet(w^{j+1} + y^{j+1}),$$

from which we define  $\ell^j \in (\mathcal{V}^j)'$ :

$$(6.2) \quad \ell^j = \begin{cases} \ell^J, & j = J \\ f^j(w^j) + R(\ell^{j+1} - f^{j+1}(w^{j+1} + y^{j+1})), & j < J. \end{cases}$$

As in FAS [34, section 5.3], injection  $R^\bullet$  coarsens the (primal) iterates, but canonical restriction  $R$  coarsens the (dual) linear functionals. Descending through the levels  $j = J, J-1, \dots, 1$  we solve the following VI problems for  $y^j \in \mathcal{D}^j$ :

$$(6.3) \quad \langle f^j(w^j + y^j), v - y^j \rangle \geq \langle \ell^j, v - y^j \rangle \quad \text{for all } v \in \mathcal{D}^j.$$

The initial iterate is  $y_{(0)}^j = 0$ ; this is admissible because  $\underline{\phi}^j \leq 0 \leq \bar{\phi}^j$ .

On ascent,  $j = 0, 1, \dots, J$ , nearly the same VI is solved, but now for  $z^j \in \mathcal{U}^j$ :

$$(6.4) \quad \langle f^j(w^j + z^j), v - z^j \rangle \geq \langle \ell^j, v - z^j \rangle \quad \text{for all } v \in \mathcal{U}^j.$$

However, the nontrivial initial iterate for this problem is found by prolonging  $z^{j-1} \in \mathcal{U}^{j-1}$  and then updating the current (i.e. down-smoothed) correction:

$$(6.5) \quad z_{(0)}^j = y^j + Pz^{j-1}.$$

An exception is that  $z_{(0)}^0 = 0$  on the coarsest level. Note  $z_{(0)}^j$  is admissible by (5.12).

Formula (6.2) for  $\ell^j$  is a classical FAS construction; compare equation (8.5b) in [7] or equation (5.3.14) in [34]. It has the following explanation, inductively on VI problems (6.3). Because the down-smoother was only approximate, problem (6.3) was not solved exactly by the finer-level correction  $y^{j+1} \in \mathcal{D}^{j+1}$ . Suppose we seek an improved correction by adding  $y \in \mathcal{D}^j$ , to give  $y^{j+1} + y \in \mathcal{D}^{j+1} + \mathcal{D}^j \subset \mathcal{V}^{j+1}$ , so that

$$(6.6) \quad \langle f^{j+1}(w^{j+1} + y^{j+1} + y), v - y \rangle \geq \langle \ell^{j+1}, v - y \rangle \quad [\text{notional}]$$

for all  $v \in \mathcal{D}^j$ . (Note  $v - y = (y^{j+1} + v) - (y^{j+1} + y)$  and that nesting  $\mathcal{V}^j \subset \mathcal{V}^{j+1}$  is assumed here.)

However, because the down-smoother has made progress,  $y$  should be approximate-able via a coarser  $j$ th-level problem generated by modifying (6.6) in 4 steps: (i) subtract the computable quantity  $f^{j+1}(w^{j+1} + y^{j+1}) \in (\mathcal{V}^{j+1})'$  from both sides, (ii) replace the relaxed residual  $\ell^{j+1} - f^{j+1}(w^{j+1} + y^{j+1})$  on the right by its restriction, (iii) replace  $w^{j+1} + y^{j+1}$  where it appears on the left by its injection, and (iv) where it appears on the left, replace  $f^{j+1}$  by the coarser discretization  $f^j$ . These steps yield a problem for the  $j$ th-level correction  $y = y^j \in \mathcal{D}^j$ :

$$(6.7) \quad \begin{aligned} & \langle f^j(R^\bullet(w^{j+1} + y^{j+1}) + y^j), v - y^j \rangle - \langle f^j(R^\bullet(w^{j+1} + y^{j+1})), v - y^j \rangle \\ & \geq \langle R(\ell^{j+1} - f^{j+1}(w^{j+1} + y^{j+1})), v - y^j \rangle, \end{aligned}$$

for all  $v \in \mathcal{D}^j$ . Though it is cluttered, this becomes VI problem (6.3) once definitions (6.1) and (6.2) are applied.

The explanation for (6.4) and (6.5) is simpler. Whether or not problem (6.3) has been exactly solved by the computed  $y^j \in \mathcal{D}^j$ , when going upward we can expand the VI problem into the larger set  $\mathcal{U}^j \supset \mathcal{D}^j$ . Inclusion (5.12) assures admissibility upward from any approximate solution to (6.4). Our current best estimate of the solution to (6.4) is  $z^j \approx y^j + Pz^{j-1} \in \mathcal{U}^j$ , so this is the initial iterate for relaxation.

These ideas come together in Algorithm 6.1, FASCD-VCYCLE, which updates  $w^J$ . The SMOOTH and SOLVE procedures are assumed to do in-place modifications of their final arguments. With `down` = 1 and `up` = 1 smoother iterations on each level, Algorithm 6.1 is a  $V(1, 1)$  cycle. The  $V(1, 0)$  cycle with `up` = 0 generalizes Algorithm 4.2 in [23] by applying FAS-type corrections and allowing any smoother. A single  $V(1, 1)$  iteration of FASCD-VCYCLE approximates an application of CD-MULT (Section 3) over CD (5.8), followed by ICD-TELE (Section 5) over inclusion (5.12), and in this sense  $V(1, 1) = V(1, 0) + V(0, 1)$ .

Regarding the storage required, if all box constraints are nontrivial then 7 vectors must be allocated on each level:  $\underline{\chi}^j, \bar{\chi}^j, \underline{\phi}^j, \bar{\phi}^j, w^j, \ell^j, y^j$ ; note vectors  $z^j$  and  $y^j$  may use the same storage. On the finest level one must also store  $\underline{\gamma}^J$  and  $\bar{\gamma}^J$ . Therefore, using  $m_j = 2^d m_{j-1}$  and a geometric series argument, the total storage is at most

$$(6.8) \quad 9m_J + 7m_{J-1} + \cdots + 7m_1 + 7m_0 \leq \left(9 + \frac{7}{2^d - 1}\right) m_J,$$

at most  $16m_J$ ,  $12m_J$ , and  $10m_J$  in dimensions  $d = 1, 2, 3$ , respectively. For comparison, a single-level method needs  $4m_J$  storage (i.e.  $\underline{\gamma}^J, \bar{\gamma}^J, \ell^J, w^J$ ). In unilateral cases the storage can be reduced at all levels.

---

**Algorithm 6.1** The FASCD V-cycle for solving VI problem (4.4).

---

```

1  FASCD-VCYCLE( $J, \ell^J, \underline{\gamma}^J, \bar{\gamma}^J; w^J$ ):
2     $\underline{\chi}^J, \bar{\chi}^J = \underline{\gamma}^J - w^J, \bar{\gamma}^J - w^J$ 
3    for  $j = J$  downto  $j = 1$ 
4       $\underline{\chi}^{j-1}, \bar{\chi}^{j-1} = R^\oplus \underline{\chi}^j, R^\ominus \bar{\chi}^j$ 
5       $\underline{\phi}^j, \bar{\phi}^j = \underline{\chi}^j - P \underline{\chi}^{j-1}, \bar{\chi}^j - P \bar{\chi}^{j-1}$ 
6       $y^j = 0$ 
7      SMOOTHdown( $\ell^j, \underline{\phi}^j, \bar{\phi}^j, w^j; y^j$ )          (VI problem (6.3) in  $\mathcal{D}^j$ )
8       $w^{j-1} = R^\bullet(w^j + y^j)$ 
9       $\ell^{j-1} = f^{j-1}(w^{j-1}) + R(\ell^j - f^j(w^j + y^j))$ 
10      $z^0 = 0$ 
11     SOLVE( $\ell^0, \underline{\chi}^0, \bar{\chi}^0, w^0; z^0$ )          (VI problem (6.4) in  $\mathcal{U}^0$ )
12     for  $j = 1$  to  $j = J$ 
13        $z^j = y^j + P z^{j-1}$ 
14       SMOOTHup( $\ell^j, \underline{\chi}^j, \bar{\chi}^j, w^j; z^j$ )          (VI problem (6.4) in  $\mathcal{U}^j$ )
15     return  $w^J + z^J$ 

```

---

**7. Implementation.** In this Section we propose a convergence criterion, construct the full multigrid (FMG) extension of Algorithm 6.1, and summarize the reduce-space Newton method used as the smoother and coarse solver.

A solution of finite-dimensional VI problem (4.4) will not generally reduce the residual  $f^J(u^J) - \ell^J$  to zero everywhere. Instead the VI is equivalent to a *mixed complementarity problem* (MCP) [19] which says, by definition, that certain conditions hold for  $u^J$  at nodes  $x_p \in \mathcal{T}^J$ . Let  $r(u^J)_p = \langle f^J(u^J) - \ell^J, \psi_p \rangle$  be the ordinary residual at  $x_p$ . If  $x_p \notin \partial_D \Omega$  then from (4.4) exactly one of these four conditions must hold:

- $\underline{\gamma}^J(x_p) < u^J(x_p) < \bar{\gamma}^J(x_p)$  and  $r(u^J)_p = 0$ ,
- $\underline{\gamma}^J(x_p) = u^J(x_p) < \bar{\gamma}^J(x_p)$  and  $r(u^J)_p \geq 0$ ,
- $\underline{\gamma}^J(x_p) < u^J(x_p) = \bar{\gamma}^J(x_p)$  and  $r(u^J)_p \leq 0$ , or
- $\underline{\gamma}^J(x_p) = u^J(x_p) = \bar{\gamma}^J(x_p)$ .

Otherwise, if  $x_p \in \partial_D \Omega$  then

- $u^J(x_p) = g_D^J(x_p)$ .

These 5 cases might be labeled *inactive*, *lower active*, *upper active*, *pinched* (both *active*), and *Dirichlet boundary*, respectively. Where *pinched* or *Dirichlet boundary* apply,  $r(u^J)_p$  can have any value.

This MCP interpretation allows us to construct expressions whose norms should approach zero. Define the Fischer-Burmeister function [3, 35] on  $a, b \in \mathbb{R}$ :

$$(7.1) \quad \phi(a, b) = a + b - \sqrt{a^2 + b^2}.$$

Observe that  $\phi$  is semi-smooth, thus continuous, and that  $\phi(a, b) = 0$  if and only if  $a, b$  are complementary, i.e.  $a \geq 0$ ,  $b \geq 0$ , and  $ab = 0$ . For any  $w^J \in \mathcal{K}^J$  denote  $\underline{g}_p = w^J(x_p) - \underline{\gamma}^J(x_p)$  and  $\bar{g}_p = \bar{\gamma}^J(x_p) - w^J(x_p)$  as the nonnegative *gaps* at  $x_p$ . Now define the *semi-smooth residual*

$$(7.2) \quad r_{\text{SS}}(w^J)_p = \begin{cases} \max \{ \phi(\underline{g}_p, r(w^J)_p), \phi(\bar{g}_p, -r(w^J)_p) \}, & x_p \notin \partial_D \Omega, \\ w^J(x_p) - g_D^J(x_p), & x_p \in \partial_D \Omega. \end{cases}$$



Straightforward modifications apply for unilaterally-constrained or unconstrained degrees of freedom, where  $\gamma^J(x_p) = -\infty$ ,  $\bar{\gamma}^J(x_p) = +\infty$ , or both. VI problem (4.4) is exactly solved by  $u^J \in \mathcal{K}^J$  if and only if  $r_{\text{SS}}(u^J) = 0$  identically.

Now suppose that Algorithm 6.1 is iterated from  $w^{J,0} \in \mathcal{K}^J$ , generating fine-level iterates  $w^{J,k} \in \mathcal{K}^J$ . Let  $\text{atol}$ ,  $\text{rtol}$ ,  $\text{stol} \geq 0$  be given absolute, relative, and step tolerances, respectively. We employ the following stopping criterion:

$$(7.3) \quad \|r_{\text{SS}}(w^{J,k})\|_2 < \text{atol} \quad \text{or} \quad \frac{\|r_{\text{SS}}(w^{J,k})\|_2}{\|r_{\text{SS}}(w^{J,0})\|_2} < \text{rtol} \quad \text{or} \quad \frac{\|\Delta w^{J,k}\|_{L^2}}{\|w^{J,k}\|_{L^2}} < \text{stol}.$$

Here  $\Delta w^{J,k} = w^{J,k} - w^{J,k-1}$ ,  $\|\cdot\|_2$  is the euclidean norm on  $\mathbb{R}^{m_J}$ , and  $\|\cdot\|_{L^2}$  is the norm on  $L^2(\Omega)$ . Defaults in our implementation (Section 8) match those of PETSc SNES [2]:  $\text{atol} = 10^{-50}$ ,  $\text{rtol} = \text{stol} = 10^{-8}$ ; see Examples below for specific settings.

In Section 8 we will show that V-cycle iterations, starting with some finest-mesh initial iterate  $w^{J,0}$  and repeated until (7.3) holds, serve as an effective solver. However, an FMG cycle, Algorithm 7.1 below and Figure 4 (right), is even better. The well-known principle [34, section 2.6] is to start on the coarsest mesh and solve the problem from any initial iterate  $w^{0,0} \in \mathcal{K}^0$ . (One may generate  $w^{0,0}$  by nodal injection and projection/truncation of  $w^{J,0}$ .) Each initial iterate on a next-finer level is generated via prolongation, but in our VI context one must also project (truncate) to the bounds to gain admissibility; see line 8 in Algorithm 7.1 below. During this “ramp” stage one approximately solves on each level using a fixed number ( $\text{rampv}$ ) of V-cycles, each down to the coarsest mesh. When the ramp is complete, one does full-depth V-cycles to convergence. When reporting iterations for the FMG cycle, “+ $n$ ” means  $n$  V-cycles were required to satisfy (7.3) after the FMG ramp, and thus “+0” means that the FMG cycle alone sufficed.

---

**Algorithm 7.1** The FASCD full multigrid (FMG) cycle for solving VI problem (4.4).

---

```

1  FASCD-FMG( $J, \ell^J, \underline{\gamma}^J, \bar{\gamma}^J$ ):
2    for  $j = J$  downto  $j = 1$ 
3       $\ell^{j-1} = R(\ell^j)$ 
4       $\underline{\gamma}^{j-1}, \bar{\gamma}^{j-1} = R^\bullet \underline{\gamma}^j, R^\bullet \bar{\gamma}^j$ 
5    choose  $w^0 \in \mathcal{K}^0$ 
6    SOLVE( $\ell^0, \underline{\gamma}^0, \bar{\gamma}^0; w^0$ )
7    for  $j = 1$  to  $j = J$ 
8       $w^j = \max \{ \underline{\gamma}^j, \min \{ \bar{\gamma}^j, Pw^{j-1} \} \} \in \mathcal{K}^j$ 
9      FASCD-VCYCLErampv( $j, \ell^j, \underline{\gamma}^j, \bar{\gamma}^j; w^j$ )
10   while not (7.3)
11     FASCD-VCYCLE( $J, \ell^J, \underline{\gamma}^J, \bar{\gamma}^J; w^J$ )
12   return  $w^J$ 
```

---

In contrast to the construction of LDCs (Section 5) for V-cycles, during the ramp standard injection is used to generate the constraints  $\underline{\gamma}^j, \bar{\gamma}^j$  on each level. This is because a full solution iterate is initially needed, not just a correction. Essentially, our choice is between (5.1), where the coarse constraint set is nonempty but then the prolonged solution may not be admissible, or (5.2), where the constraint set may be empty. We choose (5.1), with nonempty sets, but we project (truncate) pointwise to the bounds, potentially adding high-frequency noise to the initial iterate.

A large space of smoothers could be explored, but in the next Section we will only apply a fixed number of iterations of a reduced-space Newton method [2, 3], denoted as *RS Newton*. A fixed number of preconditioned Krylov iterations [11] approximately solve the arising linear systems, thus  $O(m_j)$  work is done per smoother application on level  $j$ . For the symmetric Laplacian (Example 8.1) we apply conjugate gradients (CG) with incomplete Cholesky (IC) preconditioning, but otherwise generalized minimum residual (GMRES) with incomplete LU (ILU) preconditioning is used. The coarse solver is also RS Newton, iterated to convergence using the MUMPS sparse direct linear solver [1].

**8. Results.** For  $P_1$  and  $Q_1$  elements, FASCD Algorithms 6.1 and 7.1 were implemented in Python using the Firedrake library [31], which applies solvers from the PETSc [2] library. The numerical results in this Section, which follow the Section 2 examples, focus on the scaling of iterations with mesh resolution. We will see that each V-cycle greatly reduces the residual norm, and that the application of an FMG cycle solves most of these problems to within discretization error, or nearly so.

*Example 8.1.* Consider the classical unilateral 2D Laplacian obstacle problem, namely Example 2.3 with  $p = 2$  and admissible set  $\mathcal{K} = \{v \geq \psi\}$ . We consider two cases, over square domains  $\Omega$ , with different coincidence (active) sets  $\{x \in \Omega : u(x) = \psi(x)\}$  (Figure 5). The standard “ball” problem has the unit upper hemisphere as the obstacle [11, Chapter 12]. The “spiral” problem’s obstacle is constructed to produce the coincidence set shown [23, problem 7.1.1]. For both cases we used  $P_1$  elements on a regular coarsest mesh with  $m_0 = 41$  nodes (64 triangles), and then the finest mesh had  $m_{10} \approx 3.4 \times 10^7$  nodes after 10 refinements. A single RS Newton iteration with three IC-preconditioned CG iterations was used as the smoother, and the initial iterate was  $w = \max\{0, \psi\}$ .

Table 2 shows the resulting iteration counts. For a first experiment we oversolve, with  $\text{atol} = \text{rtol} = \text{stol} = 10^{-12}$  in (7.3), to facilitate comparison to results in [23, section 7]. As expected, RS Newton as a solver shows rapidly-increasing iterations, roughly proportional to resolution. By contrast,  $V(1,1)$ -cycle iterations increase slowly, perhaps logarithmically with the resolution. For the spiral problem, [23, Figure 7.11] reports that a  $m_J \approx 5.2 \times 10^5$  problem needs approximately 25 V-cycle iterations for the best (truncated; “TNMG” and “TMMG”) monotone multilevel algorithms.<sup>3</sup> The 12 V-cycle iterations needed here for comparable resolution (8 levels) represent somewhat more arithmetic because our smoother is RS Newton using CG+IC, rather than the simpler projected Gauss-Seidel iteration.

The ball problem has a known exact solution  $u \in W^{2,\infty}(\Omega)$  [11, 32]. The measured convergence rate is  $\|u^* - u^J\|_{H^1(\Omega)} = O(h^{1.51})$ , somewhat better than  $O(h^1)$  provable from theory [15, section 5.1].

Resolution-dependent asymptotic convergence rates for V-cycles, defined as  $\rho_J = (\|r_{\text{SS}}(w^{J,k})\|_2 / \|r_{\text{SS}}(w^{J,0})\|_2)^{1/k}$  where  $w^{J,k}$  is the first iterate to satisfy (7.3), are shown in Figure 6. Both iterations and rates are similar for the ball and spiral problems; the geometric complexity of the coincidence set and free boundary minimally influences FASCD V-cycle performance. Contrast the rate of about 0.1 for 8 levels here with about 0.4 reported by [23, Figure 7.11] for TNMG/TMMG at comparable resolution. These rates are all excellent; our better rate mostly reflects a stronger

<sup>3</sup>The stopping criterion and asymptotic convergence rates in [23] are based on norm differences from a last numerical iterate with unknown accuracy. Our method directly measures satisfaction of the VI, via the residual norm  $\|r_{\text{SS}}(w)\|_2$  (Section 7).

659 smoother.

660 For the FMG cycle we instead used the defaults  $\text{rtol} = \text{stol} = 10^{-8}$ , sufficient  
 661 to reach discretization error. In Table 2 we report the number of V-cycles after the  
 662 ramp as “+ $n$ ”; a small, constant number solves the ball problem. Since each V-  
 663 cycle does the work of about eight finest-level Krylov iterations, the ball results show  
 664 nearly textbook multigrid efficiency at the highest resolutions despite the low solution  
 665 regularity. In the spiral problem, more V-cycles are needed to clean-up the remaining  
 666 (free boundary) error.

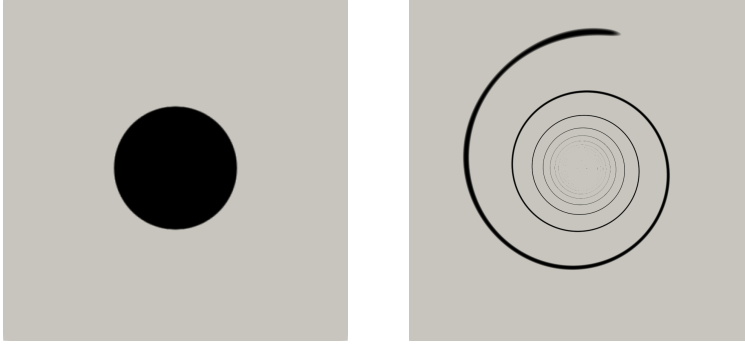


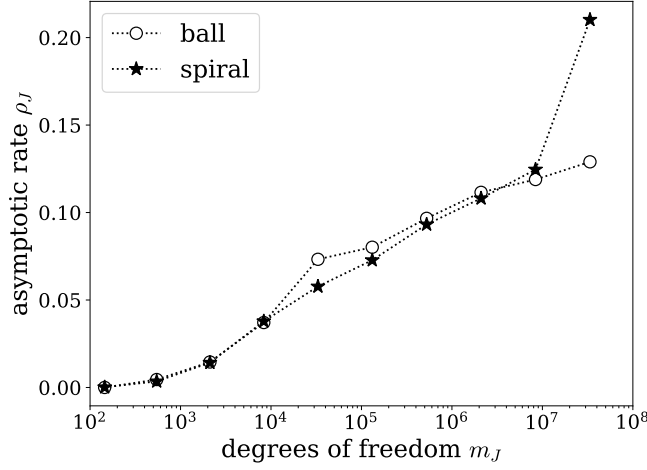
FIG. 5. Coincidence sets for the ball and spiral solutions in Example 8.1.

levels	$m_J$	ball			spiral		
		RS only	V-cycle	FMG	RS only	V-cycle	FMG
2	145	1	3	+1	4	4	+1
3	545	3	6	+2	6	5	+2
4	$2.1 \times 10^3$	6	7	+2	7	7	+3
5	$8.3 \times 10^3$	13	9	+3	11	9	+3
6	$3.3 \times 10^4$	23	11	+4	20	10	+4
7	$1.3 \times 10^5$	46	11	+3	35	11	+4
8	$5.3 \times 10^5$	90	12	+3	67	12	+4
9	$2.1 \times 10^6$	<b>X</b>	13	+2	<b>X</b>	13	+5
10	$8.4 \times 10^6$	<b>X</b>	13	+1	<b>X</b>	14	+5
11	$3.4 \times 10^7$	<b>X</b>	14	+1	<b>X</b>	18	+5

TABLE 2

Iterations for Example 8.1; see text regarding cycle types and tolerances. Runs **X** were not attempted. “+ $n$ ” for FMG denotes number of V-cycles, after the FMG cycle, to satisfy (7.3).

667 *Example 8.2.* We again consider Example 2.3, with a unilateral constraint, but  
 668 now for a nonlinear  $p$ -Laplacian [14] in one dimension. Setting  $p = 1.5$  yields a fast  
 669 diffusion with  $D = |\nabla u|^{p-2} \rightarrow \infty$  as  $|\nabla u| \rightarrow 0$ . (By contrast, Example 8.4 below  
 670 has a doubly-nonlinear operator with  $p = 4$  degenerate diffusion.) The diffusivity is  
 671 regularized, with  $|\nabla v|^p$  in (2.7) replaced by  $(\epsilon + |\nabla v|^2)^{p/2}$ , and  $\epsilon = 10^{-8}$ . We set  
 672  $\Omega = (-3, 3)$ ,  $\psi(x) = -0.2|x|$ ,  $\mathcal{K} = \{v \geq \psi\} \subset W^{1,p}(\Omega)$ , and  $\langle \ell, v \rangle = \int_{\Omega} gv$ , where  
 673  $g(x) = 1$  for  $|x| < 1$  and  $g(x) = -1$  for  $|x| > 1$ , in VI (2.1). The exact solution is easily

FIG. 6. *V-cycle asymptotic rates in Example 8.1.*

674 computed for any  $p$ ; see the codes accompanying this paper. For this experiment the  
 675 coarsest mesh has  $m_0 = 7$  nodes and the finest  $m_9 = 3073$ . The default smoother  
 676 uses three iterations of RS Newton, with LU solution of the linear systems. We set  
 677  $\text{rtol} = 10^{-6}$ ,  $\text{atol} = 10^{-12}$ , and  $\text{stol} = 0$ . Figure 7 illustrates the major steps of  
 678 a V-cycle, showing each of the coarse-correction VI subproblems and solutions; the  
 679 result  $\tilde{w}^2$  is visually close to the exact solution.

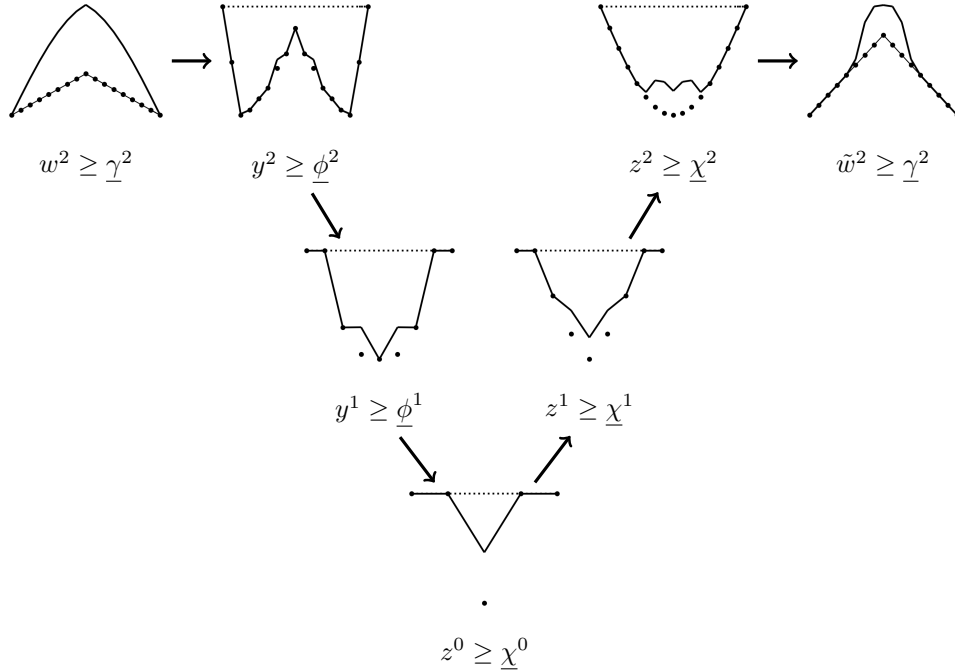


FIG. 7. *Visualization of one FASCD V-cycle iteration for  $p$ -Laplacian Example 8.2, with  $J = 3$  and a coarsest mesh of  $m_0 = 5$  vertices. Solutions (i.e.  $w^j$ ,  $y^j$ ,  $z^j$ ) are lines, obstacles ( $\underline{\gamma}^j$ ,  $\underline{\phi}^j$ ,  $\underline{\chi}^j$ ) are strong dots, and the zero function is dotted. Vertical scale varies.*

Iteration results in Table 3 show a strong contrast between  $V(1,0)$  and  $V(0,1)$  results, chosen by setting  $\text{UP} = 0$  and  $\text{DOWN} = 0$  in Algorithm 6.1, respectively. The  $V(1,0)$  cycles, essentially Algorithm 4.2 in [23] but with a stronger smoother, often do not converge. By contrast,  $V(0,1)$  cycles, which up-smooth in the larger sets  $\mathcal{U}^j$  (Section 5), are as good as the default  $V(1,1)$  cycles. FMG is even more efficient; a single cycle suffices at all resolutions. Note that measured  $L^\infty(\Omega)$  convergence is  $O(h^{1.99})$ ; compare [14].

<i>levels</i>	$m_J$	$V(1,0)$	$V(0,1)$	$V(1,1)$	FMG	$\ \text{error}\ _\infty$
2	13	3	2	2	+0	$3.3 \times 10^{-2}$
3	25	12	4	2	+0	$9.1 \times 10^{-3}$
4	49	NC	4	2	+0	$3.2 \times 10^{-3}$
5	97	14	3	3	+0	$5.5 \times 10^{-4}$
6	193	NC	3	3	+0	$1.7 \times 10^{-4}$
7	385	NC	3	3	+0	$4.7 \times 10^{-5}$
8	769	NC	3	6	+0	$9.2 \times 10^{-6}$
9	1537	NC	3	3	+0	$3.4 \times 10^{-6}$
10	3073	NC	2	5	+0	$4.1 \times 10^{-7}$

TABLE 3  
Iterations for Example 8.2. Runs “NC” did not converge after 50 iterations.

Firedrake applications can exploit the PETSc [2] library’s parallel solvers. The above Examples, which were run in serial, also run efficiently in parallel. The next two Examples apply parallel solvers and investigate the weak scaling of FMG.

*Example 8.3.* Consider the advection-diffusion VI problem in Example 2.5 with  $\Omega = (-1,1)^d$ ,  $d = 2,3$ , diffusivity  $\epsilon = 0.1$  in (2.9), and zero Dirichlet boundary conditions. The 2D problem satisfies the coercivity hypothesis, with a divergence-free velocity field  $\mathbf{X} = (7 + 5y, -5x)$ . In 3D we set  $\mathbf{X} = (7 + 5y, -5x, 2z)$  so  $\nabla \cdot \mathbf{X} \neq 0$ . The discontinuous source term  $\phi \in L^\infty(\Omega)$  satisfies  $\phi \geq 0$  in half of the domain, with positive circular patches, but values are negative in the other half; details are in the associated code. While the other Examples in this Section are unilateral, here the solution is box-constrained:  $0 \leq u \leq 1$ . Figure 8 shows coincidence sets for the 2D problem. The 3D sets are comparable in regularity and general pattern.

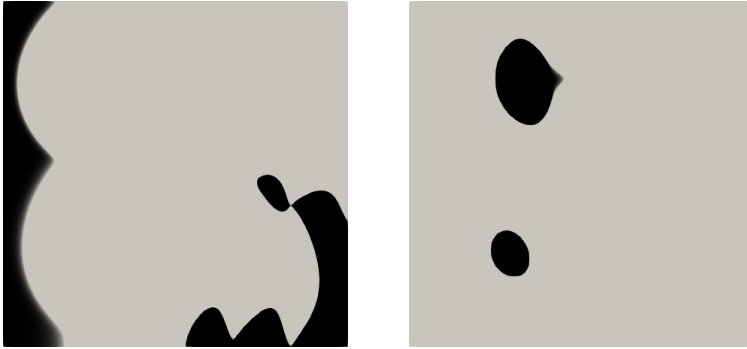


FIG. 8. Coincidence sets for the 2D results in Example 8.3:  $u = 0$  (left) and  $u = 1$  (right).

699 The 2D solver applied  $P_1$  elements on a single core, but in 3D the elements  
700 were chosen to be  $Q_1$  (hexahedra) on 16 cores. A coarse mesh with  $m_0 = 16^d$  vertices  
701 minimally-resolved the coincidence set. The local Péclet number  $\text{Pe} = \|\mathbf{X}(x, y, z)\|_2 L \epsilon^{-1}$ ,  
702 with  $L = 2$  the width of  $\Omega$ , varied from 40 to 260, and the mesh Péclet number  
703  $m_J^{-1/d} \text{Pe}$  varied further with resolution. The  $m_J \leq 121^d$  problems were numerically  
704 advection-dominated and those with  $m_J \geq 481^d$  diffusion-dominated. However, the  
705 smoother was the same in all cases: two (fixed) RS Newton iterations, with three pre-  
706 conditioned GMRES iterations. The preconditioner was the additive Schwarz method  
707 (ASM) with ILU on each process. Tolerances were set to  $\text{rtol} = 10^{-5}$  and  $\text{atol} =$   
708  $\text{stol} = 10^{-9}$ . FMG cycle results are shown in Table 4; up to memory-limited resolu-  
709 tion a couple of V-cycle iterations sufficed to satisfy (7.3).

<i>levels</i>	$m_J$	$d = 2$	$d = 3$
2	$31^d$	+1	+1
3	$61^d$	+1	+1
4	$121^d$	+1	+1
5	$241^d$	+1	+2
6	$481^d$	+1	
7	$961^d$	+2	
8	$1921^d$	+2	
9	$3841^d$	+2	

TABLE 4  
FMG cycle results for 2D ( $P_1$ , serial) and 3D ( $Q_1$ , 16 processes) solutions of Example 8.3.

710 *Example 8.4.* Recall the steady shallow ice approximation (SIA) obstacle problem  
711 in Example 2.6, in which the surface elevation is constrained to exceed the bedrock  
712 elevation,  $s \geq b$ . Let  $\Omega = (0, L)^2$  with  $L = 1800$  km. The data consist of a radial  
713 surface mass balance function  $a$  [24, equation (5.122)] and a bumpy, synthetic map  
714  $b \in C^1(\Omega)$ , with an elevation range of 1800 m; details are in the associated code. A  
715 numerical solution is shown in Figure 9, colored by surface flow speed, namely the  
716 magnitude of  $\mathbf{u} = (n+1)(n+2)^{-1} \Gamma(s-b)^{n+1} |\nabla s|^{n-1} \nabla s$  [24]. Note  $|\nabla s|$  is unbounded  
717 at the free boundary; the solution  $s$ , while continuous, has very low regularity.

718 We applied FMG using  $Q_1$  elements and a smoother of four (fixed) iterations  
719 of RS Newton (Section 7), with quadratic backtracking line search, and two (**rampv**  
720  $= 2$  in Algorithm 7.1) V-cycles per level. Three iterations of preconditioned GMRES,  
721 with an ASM+ILU preconditioner, were applied to the Newton linear systems. The  
722 coarse mesh was relatively fine, with  $m_0 = 21^2$  nodes. Because of the low regularity  
723 of the solution we used  $\text{rtol} = 2 \times 10^{-4}$  and  $\text{atol} = 10^{-8}$ . The initial iterate was  
724 zero ice:  $s = b$ . These choices generated a solver with mesh-independent iterations.

725 For a weak-scaling study, on  $P$  processes we fixed the number of degrees of freedom  
726 per process at  $m_J/P \approx 4.1 \times 10^5$  and solved with  $J+1 = 6, \dots, 11$  levels.<sup>4</sup> The results  
727 in Table 5 show some degradation in run time with increasing core counts, perhaps  
728 due to the use of single-level additive Schwarz in the Krylov iteration. Nevertheless,  
729 the finest mesh result, with  $m_J = 20481^2 = 4.1 \times 10^8$  degrees of freedom, required

<sup>4</sup>The experiments were conducted on ARCHER2, the UK national supercomputer. Each node has 16 memory channels, so a maximum of 16 cores per node were employed.

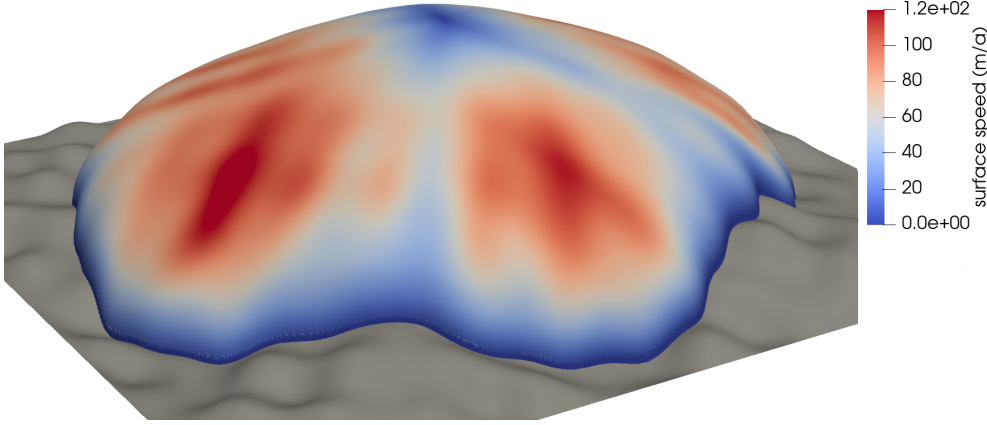


FIG. 9. *Example 8.4 solution over a bumpy bedrock topography (grey), with 100-times vertical exaggeration and surface coloring by flow speed.*

less than three minutes to solve for the steady surface elevation of an ice sheet larger in area than the current Greenland ice sheet (1.7 million  $\text{km}^2$ ), at uniform 87.5 m resolution.

$P$	levels	$m_J$	iterations	time (s)
1	6	$641^2$	+2	98
4	7	$1281^2$	+2	98
16	8	$2561^2$	+2	124
64	9	$5121^2$	+2	136
256	10	$10241^2$	+1	95
1024	11	$20481^2$	+1	177

TABLE 5

*Parallel weak scaling FMG cycle results (additional V-cycle iterations to satisfy (7.3), and wall clock time) for Example 8.4.*

**9. Discussion and outlook.** As a multilevel solver for VI problems, the FASCD method is a strategy for generating coarser-level problems which, once solved, make helpful admissible corrections within a V-cycle iteration. The method is smoother-agnostic, and our implementation within the extensible Firedrake [31] and PETSc [2] library framework will allow easy experimentation with other smoothers (projected Gauss–Seidel, semi-smooth Newton, interior-point, etc.), beyond the active-set Newton method chosen for demonstration here. For smoothers of Newton-Krylov type one could also add linear geometric or algebraic multigrid preconditioning [34] for the linear Newton step problems, instead of our simpler choice of incomplete factorization. In a different direction, a restructured multilevel CD approach which applies the additive/parallel CD iteration [32] might be considered, in pursuit of a VI algorithm analogous to the BPX multigrid method for PDEs [4]. In any case, the performance observed in Section 8 is already excellent on the tested examples.

**Code availability.** The software used to produce the results in Section 8 is archived at tag v1.0 in the repository <https://bitbucket.org/pefarrell/fascd/> and at doi:10.5281/zenodo.10476845. We used Firedrake master revision c5e939dde.

## REFERENCES

- [1] P. R. AMESTOY, I. S. DUFF, J. KOSTER, AND J.-Y. L'EXCELLENT, *A fully asynchronous multi-frontal solver using distributed dynamic scheduling*, SIAM Journal on Matrix Analysis and Applications, 23 (2001), pp. 15–41.
- [2] S. BALAY AND 34 OTHERS, *PETSc/TAO users manual*, Tech. Report ANL-21/39 - Revision 3.19, Argonne National Laboratory, 2023.
- [3] S. BENSON AND T. MUNSON, *Flexible complementarity solvers for large-scale applications*, Optimization Methods and Software, 21 (2006), pp. 155–168.
- [4] J. H. BRAMBLE, J. E. PASCIAK, AND J. XU, *Parallel multilevel preconditioners*, Mathematics of computation, 55 (1990), pp. 1–22.
- [5] A. BRANDT, *Multi-level adaptive solutions to boundary-value problems*, Math. Comp., 31 (1977), pp. 333–390.
- [6] A. BRANDT AND C. CRYER, *Multigrid algorithms for the solution of linear complementarity problems arising from free boundary problems*, SIAM J. Sci. Stat. Comput., 4 (1983), pp. 655–684.
- [7] A. BRANDT AND O. LIVNE, *Multigrid Techniques: 1984 Guide with Applications to Fluid Dynamics*, SIAM Press, Philadelphia, revised ed., 2011.
- [8] P. BRUNE, M. KNEPLEY, B. SMITH, AND X. TU, *Composing scalable nonlinear algebraic solvers*, SIAM Rev., 57 (2015), pp. 535–565.
- [9] E. BUELER, *Stable finite volume element schemes for the shallow ice approximation*, J. Glaciol., 62 (2016), pp. 230–242.
- [10] E. BUELER, *Conservation laws for free-boundary fluid layers*, SIAM J. Appl. Math., 81 (2021), pp. 2007–2032, <https://doi.org/10.1137/20M135217X>.
- [11] E. BUELER, *PETSc for Partial Differential Equations: Numerical Solutions in C and Python*, SIAM Press, Philadelphia, 2021.
- [12] C. CARSTENSEN, *Clément interpolation and its role in adaptive finite element error control*, in Partial Differential Equations and Functional Analysis: The Philippe Clément Festschrift, E. Koelink, ed., vol. 168 of Operator Theory: Advances and Applications, Birkhäuser Basel, 2006, ch. 2, pp. 27–43, <https://doi.org/10.1007/3-7643-7601-5>.
- [13] J. CHANG AND K. B. NAKSHATRALA, *Variational inequality approach to enforcing the non-negative constraint for advection–diffusion equations*, Comput. Methods Appl. Mech. Eng., 320 (2017), pp. 287–334.
- [14] H. J. CHOE AND J. L. LEWIS, *On the obstacle problem for quasilinear elliptic equations of  $p$ -Laplacian type*, SIAM J. Math. Anal., 22 (1991), pp. 623–638.
- [15] P. CIARLET, *The Finite Element Method for Elliptic Problems*, SIAM Press, Philadelphia, 2002. Reprint of the 1978 original.
- [16] I. EKELAND AND R. TEMAM, *Convex Analysis and Variational Problems*, North-Holland, Amsterdam, 1976.
- [17] H. C. ELMAN, D. J. SILVESTER, AND A. J. WATHEN, *Finite Elements and Fast Iterative Solvers: with Applications in Incompressible Fluid Dynamics*, Oxford University Press, Oxford, UK, 2nd ed., 2014.
- [18] L. C. EVANS, *Partial Differential Equations*, Graduate Studies in Mathematics, American Mathematical Society, Providence, 2nd ed., 2010.
- [19] F. FACCHINEI AND J.-S. PANG, *Finite-Dimensional Variational Inequalities and Complementarity Problems*, vol. 1, Springer, 2003.
- [20] P. E. FARRELL, M. CROCI, AND T. M. SUROWIEC, *Deflation for semismooth equations*, Optimization Methods and Software, 35 (2019), pp. 1248–1271, <https://doi.org/10.1080/10556788.2019.1613655>.
- [21] P. E. FARRELL AND J. R. MADDISON, *Conservative interpolation between volume meshes by local Galerkin projection*, Computer Methods in Applied Mechanics and Engineering, 200 (2011), pp. 89–100, <https://doi.org/10.1016/j.cma.2010.07.015>.
- [22] M. C. FERRIS AND J.-S. PANG, *Engineering and economic applications of complementarity problems*, SIAM Rev., 39 (1997), pp. 669–713.
- [23] C. GRÄSER AND R. KORNUBER, *Multigrid methods for obstacle problems*, J. Comput. Math., 27 (2009), pp. 1–44.
- [24] R. GREVE AND H. BLATTER, *Dynamics of Ice Sheets and Glaciers*, Advances in Geophysical



- and Environmental Mechanics and Mathematics, Springer, Berlin, Germany, 2009.
- [25] M. HINTERMÜLLER AND I. KOPACKA, *A smooth penalty approach and a nonlinear multigrid algorithm for elliptic MPECs*, Computational Optimization and Applications, 50 (2011), pp. 111–145.
  - [26] G. JOUVET AND E. BUELER, *Steady, shallow ice sheets as obstacle problems: well-posedness and finite element approximation*, SIAM J. Appl. Math., 72 (2012), pp. 1292–1314.
  - [27] G. JOUVET AND C. GRÄSER, *An adaptive Newton multigrid method for a model of marine ice sheets*, J. Comput. Physics, 252 (2013), pp. 419–437.
  - [28] B. KEITH AND T. M. SUROWIEC, *Proximal Galerkin: a structure-preserving finite element method for pointwise bound constraints.*, 2023, <https://doi.org/10.48550/arXiv.2307.12444>.
  - [29] D. KINDERLEHRER AND G. STAMPACCHIA, *An Introduction to Variational Inequalities and their Applications*, Academic Press, New York, 1980.
  - [30] R. KORNUBER, *Monotone multigrid methods for elliptic variational inequalities*, Numer. Math., 69 (1994), pp. 167–184.
  - [31] F. RATHGEBER, D. A. HAM, L. MITCHELL, M. LANGE, F. LUPORINI, A. T. T. McRAE, G.-T. BERCEA, G. R. MARKALL, AND P. H. J. KELLY, *Firedrake: automating the finite element method by composing abstractions*, ACM Trans. Math. Softw., 43 (2016), pp. 24:1–24:27.
  - [32] X.-C. TAI, *Rate of convergence for some constraint decomposition methods for nonlinear variational inequalities*, Numer. Math., 93 (2003), pp. 755–786.
  - [33] X.-C. TAI AND P. TSENG, *Convergence rate analysis of an asynchronous space decomposition method for convex minimization*, Math. Comput., 71 (2002), pp. 1105–1135.
  - [34] U. TROTTEBERG, C. W. OOSTERLEE, AND A. SCHULLER, *Multigrid*, Elsevier, Oxford, UK, 2001.
  - [35] M. ULBRICH, *Semismooth Newton Methods for Variational Inequalities and Constrained Optimization Problems in Function Spaces*, SIAM Press, Philadelphia, 2011.
  - [36] J. XU, *Iterative methods by space decomposition and subspace correction*, SIAM Rev., 34 (1992), pp. 581–613.